Density-functional formulation of the generalized pseudopotential theory. II

John A. Moriarty
University of Cincinnati, ML 30, Cincinnati, Ohio 45221
and Lawrence Livermore National Laboratory, University of California,
*Livermore, California 94550**
(Received 1 March 1982)

The density-functional formulation of the generalized pseudopotential theory (GPT) set forth in paper I of this set is recast in an optimum representation and more widely applied to empty- and filled-*d*-band metals. Optimization is achieved by making the most advantageous separation possible of (i) the hybridization potential into volume-dependent ($\Delta_{\rm vol}$) and structure-dependent ($\Delta_{\rm struc}$) parts, and (ii) the nonuniform component of the valence-electron density into screening and orthogonalization-hole contributions. The resulting new definitions of these quantities permit the entire contribution of $\Delta_{\rm struc}$ to the total energy to be folded into the original framework of the theory, where $\Delta_{\rm struc}$ was neglected. The energy-wave-number characteristic $F(q)$ and overlap potential $v_{\rm ol}(r)$ then assume simpler and more computationally efficient forms, in which certain large numerical cancellations otherwise inherent in the calculation of physical properties are eliminated. The new representation also makes clearer the ranges of applicability of the empty- and filled-*d*-band limits of the theory. The optimized GPT is shown to provide an excellent description of the group-II*A* metals Ca and Sr in the empty-*d*-band limit and of the group-II*B* metals Zn and Cd in the filled-*d*-band limit. Somewhat surprisingly, however, a filled-*d*-band treatment is found *not* to be adequate in the noble metals because the number of electrons effectively emptied out of the *d* states through hybridization ($\sim\frac{1}{2}$ electron/atom) is not small relative to the nominal valence (1 electron/atom). It is further shown that a much more accurate description of the noble metals can be expected by allowing the *d* states to unfill and a self-consistent valence to be achieved in zero order, and the first steps towards implementing the partially-filled-*d*-band limit of the GPT are considered here. Finally, extensive applications of the optimized GPT that we have made on the band structure, cohesion, liquid-metal transport, lattice dynamics, and structural phase stability in 22 simple and *d*-band metals are summarized and compared with both experiment and the density-functional calculations of Moruzzi, Janak, and Williams.

I. INTRODUCTION

Over the past ten years we have sought to extend the spirit of simple-metal pseudopotential perturbation theory to *d*-band metals in both a systematic and rigorous way.[1–8] For metals near the beginning and end of the transition series, with empty and filled *d*-bands, respectively, our work has developed into a first-principles, generalized pseudopotential theory (GPT) whose formal structure is a direct generalization of the conventional nonlocal pseudopotential theory of simple metals.[9,10] This paper, together with Ref. 7 (paper I of this set), represent our most extensive efforts to refine and widely apply the GPT to empty- and filled-*d*-band metals.

In paper I, we completely rederived the internal details of the GPT beginning from the Kohn-Sham density-functional formalism.[11] We showed that to a good approximation in *d*-band metals the total self-consistent potential $V(\vec{r})$, including its inherently nonlinear exchange and correlation contributions, can be written in rigid-ion form, that is, as a sum of position-independent, intra-atomic potentials:

$$V(\vec{r})=\sum_i v(\vec{r}-\vec{R}_i)\ , \tag{1}$$

where $\vec{R}_i$ is the position of the ith nucleus. This allowed us to rigorously separate volume-dependent and structure-dependent quantities and to obtain, as desired, the electron density in the form

$$n(\vec{r})=n_{\rm unif}+\sum_i n_{\rm core}(\vec{r}-\vec{R}_i)+\sum_{\vec{q}}{}' S(\vec{q})\delta n_{\rm val}(q)e^{i\vec{q}\cdot\vec{r}}\ , \tag{2}$$

where $S(\vec{q})$ is the usual structure factor and the prime on the latter sum excludes the $q=0$ term, and the total energy in the form

$$E_{\rm tot}=E_0(\Omega_0)+E_{\rm es}(Z^*)+N\sum_{\vec{q}}{}' \mid S(\vec{q})\mid^2 F(q) + \tfrac{1}{2}\sum_{i,j}{}' v_{\rm ol}(\mid \vec{R}_i-\vec{R}_j\mid), \quad (3)$$

where $E_{\rm es}$ is the electrostatic energy of point ions of charge Z^*e in a compensating uniform background and the prime on the final sum excludes the $\vec{R}_i=\vec{R}_j$ term. The uniform density $n_{\rm unif}$, core density $n_{\rm core}$, and oscillatory valence density $\delta n_{\rm val}$, as well as the energy-wave-number characteristic F, d-state overlap potential $v_{\rm ol}$, and volume energy term E_0, are all *structure-independent characteristic functions* which can either be calculated directly or evaluated in a relatively straightforward manner through matrix elements of a nonlocal pseudopotential w_0 and a d-state hybridization potential Δ. Moreover, in the process of developing Eq. (3), new structure-dependent total energy terms were uncovered, which arise from the small structure-dependent part, $\Delta_{\rm struc}$, of the total d-state hybridization potential

$$\Delta=\Delta_{\rm vol}+\Delta_{\rm struc}, \quad (4)$$

where $\Delta_{\rm vol}$ is the larger volume contribution. This led to significantly modified forms for both the energy-wave-number characteristic and d-state overlap potential.

In this paper we complete the work begun in paper I with a number of additional major refinements, extensions, and new applications of the GPT. In Sec. II, we first discuss an alternative, and what we now believe is an optimum representation of the theory as applied to filled- and empty-d-band metals. This optimum representation, which largely arises out of an internal mathematical transformation of the results obtained in paper I, is significant in several respects. First, the characteristic functions can be defined and written in more compact and transparent forms. This adds, for example, considerable insight into the role of the structure dependence of the hybridization and suggests a general algorithm for treating its effect in all d-band metals, including transition metals. Second, the optimum GPT is more computationally efficient as a whole and slightly more accurate. Certain large cancellations which occur in the calculation of physical properties, and which were achieved only numerically in paper I, are now, in effect, accomplished algebraically. Finally, the new representation makes clearer the general limits of applicability of the theory and additional evidence supporting its important significance to group-II*A* (e.g., Ca) and group-II*B* (e.g., Zn) metals is presented.

In Sec. III, the scope of the studies begun in paper I is broadened to include full consideration of the difficult case of the noble metals, with new and very revealing results. In contrast to early expectations[1,3,12] and also to recent related work by Dagens and co-workers,[13–17] we find that the noble metals can only be treated in a marginally acceptable way as metals having filled d bands, with several *ad hoc* adjustments in the GPT required. This limitation arises because the actual unfilling of the d bands through hybridization in these metals is *not* quantitatively small ($\sim\frac{1}{2}$ electron/atom) relative to the nominal sp-band occupation (1 electron/atom). We show that a much more accurate description of the noble metals can be expected by treating these materials as transition metals having partially filled d bands and the first steps towards a complete theory of partially-filled-d-band metals are considered here.

In Sec. IV, additional applications of the optimized GPT are summarized and discussed. These include detailed comparisons on band structure and electron density with the full density-functional band calculations of Moruzzi, Janak, and Williams (MJW),[18] as well as new results on cohesion, liquid-metal transport, lattice dynamics, and structural phase stability in 22 metals. Concluding remarks are given in Sec. V.

II. OPTIMUM FORM OF THE THEORY

To arrive at the optimum representation of the GPT, it is first necessary to reexamine the details of both the hybridization potential Δ and the oscillatory valence density $\delta n_{\rm val}$. With regard to the former, we focus on the separation of Δ into a volume-dependent and a structure-dependent contribution, as in Eq. (4). We now take advantage of the fact that this separation is not totally unique and in practice can be done in two closely related but distinct ways depending on how the free-electron terms are handled. By definition, the total hybridization potential acting on a localized d state $|\phi_d\rangle$ is[19]

$$\Delta=\delta V-\langle\phi_d\mid\delta V\mid\phi_d\rangle, \quad (5)$$

where δV is the difference in potential between the reference Hamiltonian H_0 of which $|\phi_d\rangle$ is an

eigenstate and the total metal Hamiltonian $H=T+V$. The reference Hamiltonian is established by our so-called zero-order pseudoatom construction, as discussed previously[6,7] and briefly reviewed in Sec. III, so that

$$\delta V(\vec{r})=v_{\rm loc}(r)+v_{\rm pa}(r)-V(\vec{r}) , \tag{6}$$

where the total pseudoatom potential $v_{\rm pa}$ is that arising from a single-site component of the zero-order charge density in the metal and $v_{\rm loc}$ is an additional localization potential which tailors the spatial tail of $\phi_d(\vec{r})$ in such a way as to minimize the effective strength of Δ. In paper I, the volume component of Δ (there denoted by $\Delta_{\rm pa}$) was defined as that arising from $v_{\rm loc}$ and the structure component (denoted by $\Delta'_{\rm struc}$) as that arising from $v_{\rm pa}-V$. Although this division is a natural one, it is not optimum due to the fact that $v_{\rm pa}-V$ actually contains a small structure-independent part, $\delta V_{\rm unif}$, which is the difference between the single-site, uniform-electron-gas potential $v_{\rm unif}$ [Eq. (29) of paper I] and the total uniform-electron-gas potential $V_{\rm unif}$:

$$\delta V_{\rm unif}=v_{\rm unif}-V_{\rm unif} . \tag{7}$$

In paper I, $\delta V_{\rm unif}$ was expressed as the difference between two large structure-dependent terms. This led to Eq. (31) of paper I for δV. In analyzing the principal hybridization matrix element $\langle \vec{k} \mid \Delta \mid \phi_d \rangle$ into volume and structure components, however, the more desirable alternative is to absorb $\delta V_{\rm unif}$ directly into the volume component of δV and write

$$\delta V=\delta V_{\rm vol}+\delta V_{\rm struc} , \tag{8}$$

where

$$\delta V_{\rm vol}=v_{\rm loc}+\delta V_{\rm unif} \tag{9}$$

and

$$\delta V_{\rm struc}=v_{\rm pa}-V-\delta V_{\rm unif} , \tag{10}$$

with $\Delta_{\rm vol}$ and $\Delta_{\rm struc}$ defined as

$$\Delta_{\rm vol}=\delta V_{\rm vol}-\langle \phi_d \mid \delta V_{\rm vol} \mid \phi_d \rangle \tag{11}$$

and

$$\Delta_{\rm struc}=\delta V_{\rm struc}-\langle \phi_d \mid \delta V_{\rm struc} \mid \phi_d \rangle , \tag{12}$$

respectively. Then all uniform-electron-gas contributions are removed from $\delta V_{\rm struc}$, and $\delta V_{\rm unif}$ in Eq. (9) can be calculated as

$$\delta V_{\rm unif}(r)=\begin{cases} 0, & r<R_{\rm WS} \\ \dfrac{Ze^2}{r}-\dfrac{1}{2}\dfrac{Ze^2}{R_{\rm WS}}(3-r^2/R_{\rm WS}^2), & r>R_{\rm WS} \end{cases} , \tag{13}$$

where Z is the valence and $R_{\rm WS}$ the Wigner-Seitz radius of the metal. Equations (5)–(13) remain exact and only a redefinition of terms has occurred at this point.

The principal significance of the new assignment of volume and structure contributions comes in the elimination of the otherwise large cancellations introduced into $\delta V_{\rm struc}$ and hence ultimately into the characteristic functions F and $v_{\rm ol}$. With the aid of Eqs. (19) and (25) of paper I, $\delta V_{\rm struc}$ can now be reduced to the form

$$\delta V_{\rm struc}(\vec{r})=-\sum_{j\neq 0}{}' v_{\rm ion}(\vec{r}-\vec{R}_j) - \sum_{\vec{q}}{}' S(\vec{q})\frac{4\pi e^2}{q^2}[1-G(q)] \times \delta n_{\rm val}(q)e^{i\vec{q}\cdot\vec{r}} , \tag{14}$$

where G is an exchange-correlation function [see Eq. (26) and surrounding discussion of paper I] and $v_{\rm ion}$ is the ionic potential of a single zero-order pseudoatom:

$$v_{\rm ion}(r)=\frac{Z}{Z_a}v_{\rm nuc}(r)+v_{\rm nuc\text{-}core}(r) , \tag{15}$$

with

$$v_{\rm nuc\text{-}core}(r)=\frac{Z_a-Z}{Z_a}v_{\rm nuc}(r)+v_{\rm core}(r)+v_{\rm xc}(r) , \tag{16}$$

Here, as in paper I, Z_a is the atomic number of the metal under consideration, $v_{\rm nuc}$ and $v_{\rm core}$ are the direct Coulomb potentials arising from the nucleus and filled inner-core and d states, respectively, and $v_{\rm xc}$ is the appropriate valence-core exchange-correlation potential [Eq. (17) of paper I].

To take full advantage of Eq. (14) for $\delta V_{\rm struc}$, it turns out to be necessary to redefine the components of $\delta n_{\rm val}$. This electron density contains both orthogonalization-hole and screening contributions, but the actual distinction between the two is also somewhat nonunique. In all of our previous work[1–8] the separation has been handled by taking the orthogonalization-hole contribution in its fami-

liar simple-metal form, so that in real space[19]

$$\delta n^0_{\rm oh}(\vec{r})=\frac{Z^*_0-Z}{Z}n_{\rm unif}+\sum_i n^0_{\rm oh}(\vec{r}-\vec{R}_i)\ , \tag{17}$$

where the hole surrounding each nucleus corresponds to a density

$$n^0_{\rm oh}(\vec{r})=-\frac{2\Omega_0}{(2\pi)^3}\int_{k<k_F}[\langle\vec{r}\,|p\,|\,\vec{k}\rangle\langle\vec{k}\,|\,\vec{r}\rangle+\text{c.c.} -\langle\vec{r}\,|p\,|\,\vec{k}\rangle\langle\vec{k}\,|p\,|\,\vec{r}\rangle]d\vec{k}\ , \tag{18}$$

with p the single-site, inner-core, and d-state projection operator

$$p=\sum_{\alpha=c,d}|\phi_\alpha\rangle\langle\phi_\alpha|\ , \tag{19}$$

and where Z^*_0 is the effective valence of the metal

$$Z^*_0=Z-\int n^0_{\rm oh}(\vec{r})d\vec{r} =Z+\frac{2\Omega_0}{(2\pi)^3}\int_{k<k_F}\langle\vec{k}\,|p\,|\,\vec{k}\rangle d\vec{k}\ . \tag{20}$$

[The $\vec{k}$-space integration region in Eqs. (18) and (20) is inside the free-electron Fermi sphere of radius k_F.] The remaining terms in $\delta n_{\rm val}$ were then included, by default, into the screening electron density $\delta n^0_{\rm scr}$ [Eq. (53) of paper I]. It has subsequently become clear, however, that one contribution to $\delta n^0_{\rm scr}$ has a definite orthogonalization-hole-like nature, and it is now advantageous to redefine the orthogonalization hole for a single site to absorb this contribution:

$$n_{\rm oh}(\vec{r})=n^0_{\rm oh}(\vec{r})\mp\frac{2\Omega_0}{(2\pi)^3}\int_{k\gtrless k_F}h_2(\vec{k},\vec{r})d\vec{k}\ , \tag{21}$$

where

$$h_2(\vec{k},\vec{r})=\sum_d\left[\frac{\langle\vec{r}\,|\,\phi_d\rangle\langle\phi_d\,|\,\Delta_{\rm vol}\,|\,\vec{k}\rangle[\langle\vec{k}\,|\,\phi_d\rangle\langle\phi_d\,|\,\vec{r}\rangle-\langle\vec{k}\,|\,\vec{r}\rangle]}{\epsilon_{\vec{k}}-E^{\rm vol}_d}+\text{c.c.} +\frac{\langle\vec{r}\,|\,\phi_d\rangle\langle\phi_d\,|\,\Delta_{\rm vol}\,|\,\vec{k}\rangle\langle\vec{k}\,|\,\Delta_{\rm vol}\,|\,\phi_d\rangle\langle\phi_d\,|\,\vec{r}\rangle}{(\epsilon_{\vec{k}}-E^{\rm vol}_d)^2}\right], \tag{22}$$

with $\epsilon_{\vec{k}}=\hbar^2k^2/2m$. In Eq. (21), as well as in appropriate equations below, the integration region is restricted to $k>k_F$ with the top (minus) sign for filled-d-band metals and to $k<k_F$ with the bottom (plus) sign for empty-d-band metals. The effect of $h_2(\vec{k},\vec{r})$ is to deplete additional election density from the d region at the outer edge of the core in the filled-d-band case, while to add electron density to this region in the empty-d-band case. This is illustrated in Figs. 1 and 2 where $n_{\rm oh}$ and $n^0_{\rm oh}$ are compared for the cases of Zn and Ca, respectively.

With the orthogonalization hole defined by Eq. (21), one then has

$$\delta n_{\rm val}=\delta n_{\rm oh}+\delta n_{\rm scr}\ , \tag{23}$$

with

$$\delta n_{\rm oh}(\vec{r})=\frac{Z^*-Z}{Z}n_{\rm unif}+\sum_i n_{\rm oh}(\vec{r}-\vec{R}_i)\ , \tag{24}$$

where the new effective valence of the metal is

$$Z^*=Z-\int n_{\rm oh}(\vec{r})d\vec{r} =Z^*_0\pm\frac{2\Omega_0}{(2\pi)^3}\int_{k\gtrless k_F}h_2(\vec{k},\vec{q}=0)d\vec{k}\ , \tag{25}$$

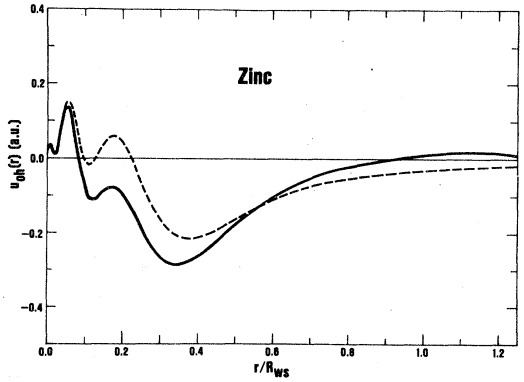

FIG. 1. Radial orthogonalization-hole density $u_{\rm oh}(r)=4\pi r^2 n_{\rm oh}(r)$ for Zn, as calculated from the present definition Eq. (21) (solid curve) and from the simple-metal definition Eq. (18) (dashed curve).

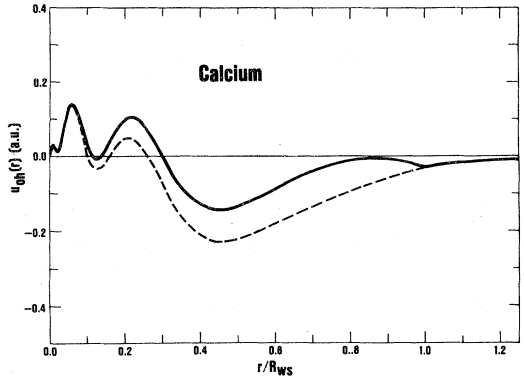

FIG. 2. Radial orthogonalization hole density u_{oh} for Ca, with the notation the same as Fig. 1.

and

$$\delta n_{scr}(\vec{r})=\sum_{\vec{q}}{}' S(\vec{q})n_{scr}(q)e^{i\vec{q}\cdot\vec{r}} , \tag{26}$$

where

$$n_{scr}(q)=n^0_{scr}(q)\pm\frac{2}{(2\pi)^3}\int_{k\gtrless k_F} h_2(\vec{k},\vec{q})d\vec{k} . \tag{27}$$

In Eqs. (25) and (27), $h_2(\vec{k},\vec{q})$ is the Fourier transform

$$h_2(\vec{k},\vec{q})=\int h_2(\vec{k},\vec{r})e^{-i\vec{q}\cdot\vec{r}}d\vec{r} , \tag{28}$$

as in Eq. (55) of paper I.[19] Note, however, that Δ_{pa} and E_d^{pa} in paper I are here replaced by Δ_{vol} and E_d^{vol}, respectively, encumbering the extra volume contribution of δV_{unif}, as discussed above for Δ_{vol}. The quantity E_d^{vol} is precisely defined as the structure-independent component of the total d-state energy expectation value

$$E_d=\langle\phi_d\,|\,T+V\,|\,\phi_d\rangle=E_d^{vol}+E_d^{struc} , \tag{29}$$

with

$$E_d^{vol}=\langle\phi_d\,|\,T+v_{pa}\,|\,\phi_d\rangle+\langle\phi_d\,|\,v_{loc}-\delta V_{vol}\,|\,\phi_d\rangle$$
$$=E_d^{pa}-\langle\phi_d\,|\,\delta V_{unif}\,|\,\phi_d\rangle , \tag{30}$$

and

$$E_d^{struc}=-\langle\phi_d\,|\,\delta V_{struc}\,|\,\phi_d\rangle . \tag{31}$$

The quantitative significance of the new definitions of Z^* and n_{oh} can be appreciated by comparing Z^* and Z_0^*. This is done in Table I for 22 nontransition metals. As in paper I, we treat the heavy group-I*A* and -II*A* elements (K, Rb, Cs, Ca, Sr, and Ba) as empty-*d*-bands metals ($Z^*<Z_0^*$), the group-I*B* and -II*B* metals (Cu, Ag, Au, Zn, Cd, and Hg) as filled-*d*-band metals ($Z^*>Z_0^*$), and the

TABLE I. Magnitudes of the new and old effective valences Z^* and Z_0^*, as obtained from Eqs. (25) and (20), respectively, for 22 nontransition metals.

Metal	Z	Z^*	Z_0^*	$(Z^*-Z_0^*)/Z$	$(Z^*-Z)/Z$
Li	1	1.0859	1.0859	0.0	0.086
Na	1	1.0877	1.0877	0.0	0.088
K	1	1.1440	1.1638	−0.020	0.144
Rb	1	1.1743	1.1994	−0.025	0.174
Cs	1	1.2243	1.2597	−0.035	0.224
Be	2	2.1515	2.1515	0.0	0.076
Mg	2	2.1849	2.1849	0.0	0.092
Ca	2	2.1332	2.3939	−0.130	0.067
Sr	2	2.2832	2.4961	−0.106	0.142
Ba	2	2.4905	2.7745	−0.142	0.245
Cu	1	1.5618	1.1691	0.393	0.562
Ag	1	1.4626	1.2234	0.239	0.463
Au	1	1.5840	1.2769	0.307	0.584
Zn	2	2.2737	2.2417	0.016	0.137
Cd	2	2.3589	2.3340	0.012	0.179
Hg	2	2.4374	2.4005	0.018	0.219
Al	3	3.2619	3.2619	0.0	0.087
Ga	3	3.2479	3.2479	0.0	0.083
In	3	3.3887	3.3887	0.0	0.130
Tl	3	3.4670	3.4670	0.0	0.156
Sn	4	4.4095	4.4095	0.0	0.102
Pb	4	4.4957	4.4957	0.0	0.124

remaining elements as simple metals ($Z^*=Z_0^*$). Two quantities of special interest here are the relative amount of additional charge depleted from the d region of each core,

$$(Z^*-Z_0^*)/Z\ ,$$

and the relative magnitude of the new orthogonalization hole,

$$(Z^*-Z)/Z\ .$$

It can be seen from Table I that the former quantity is less than 0.15 except in the case of the noble metals, where it becomes several times larger. Likewise, $(Z^*-Z)/Z$ remains acceptably small in all but Cu, Ag, and Au, increasing to something on the order of 0.5 for these metals. The latter is very revealing and, in point of fact, symptomatic of the basic difficulty one has in treating the noble metals as having completely filled d bands. The large $(Z^*-Z)/Z$ represents a relatively large redistribution of d-electron charge from inside to outside the outer-core region, which is physically just the effect of unfilling the d bands. The practical problem in the noble metals comes in trying to accommodate this sizable shift in terms of the (assumed small) first-order density $\delta n_{\rm val}$.

An interesting connection can also be made between our new definition of the orthogonalization hole and the concept of the depletion hole in model potential theory,[20] which has recently been generalized to empty- and filled-d-band metals by Dagens.[13–15] In model potential theory, the magnitude of the depletion hole is related to the first energy derivative of the model potential. In the GPT, the appropriate analog of Dagens's so-called resonant model potential is the energy-dependent pseudopotential

$$\begin{aligned} w(E)=v&+\sum_{\alpha=c,d}(E-E_\alpha^{\rm vol})\,|\,\phi_\alpha\rangle\langle\phi_\alpha\,| \\ &+\sum_d(\Delta_{\rm vol}\,|\,\phi_d\rangle\langle\phi_d\,|+{\rm H.c.}) \\ &+\sum_d\frac{\Delta_{\rm vol}\,|\,\phi_d\rangle\langle\phi_d\,|\,\Delta_{\rm vol}}{(E-E_d^{\rm vol})}\ , \end{aligned} \tag{32}$$

in which case, for example, the matrix element $\langle\vec{k}+\vec{q}\,|\,w(\epsilon_{\vec{k}})\,|\,\vec{k}\rangle$ is the form factor on the constant energy surface $E=\epsilon_{\vec{k}}$. Taking the first energy derivative of Eq. (32), one obtains

$$\frac{dw(E)}{dE}=p-\sum_d\frac{\Delta_{\rm vol}\,|\,\phi_d\rangle\langle\phi_d\,|\,\Delta_{\rm vol}}{(E-E_d^{\rm vol})^2}\ . \tag{33}$$

Properly summing $\langle\vec{k}\,|\,dw(\epsilon_{\vec{k}})/dE\,|\,\vec{k}\rangle$ over $\vec{k}$ states then exactly reproduces Z^*-Z:

$$Z^*-Z=\frac{2\Omega_0}{(2\pi)^3}\left[\int_{k<k_F}\langle\vec{k}\,|\,p\,|\,\vec{k}\rangle d\vec{k}\pm\int_{k\gtrless k_F}\sum_d\frac{\langle\vec{k}\,|\,\Delta_{\rm vol}\,|\,\phi_d\rangle\langle\phi\,|\,\Delta_{\rm vol}\,|\,\vec{k}\rangle}{(\epsilon_{\vec{k}}-E_d^{\rm vol})^2}d\vec{k}\right]\ . \tag{34}$$

In Dagens's approach, the second term in Eq. (34) becomes the quantity he calls $-Z_{\rm dpl}$, so that the precise relation is $Z^*-Z_0^*=-Z_{\rm dpl}$. It is noteworthy, however, that the values Dagens has calculated[13,14] for $-Z_{\rm dpl}$ in the noble metals and Ca differ substantially from $Z^*-Z_0^*$ in Table I. In the noble metals his $-Z_{\rm dpl}$ is actually several times larger than our $Z^*-Z_0^*$ (compounding the basic difficulty mentioned above), while in Ca his value is about one-half of ours. As discussed in Sec. III, the reasons for this appear to be related to Dagens's modeling of the hybridization integral $\langle\vec{k}\,|\,\Delta_{\rm vol}\,|\,\phi_d\rangle$.

Equally as important as the insight offered by our new definition of the orthogonalization hole is the formal significance of Eq. (21) for $n_{\rm oh}$ to the internal structure of the GPT as a whole. Specifically, there is now an intimate relationship between $n_{\rm oh}$ and the structure-dependent part of the hybridization potential when $\delta V_{\rm struc}$ is given by Eq. (14). As shown in Appendix A, the entire contribution of $\Delta_{\rm struc}$ to the second-order total energy reduces to the simple electrostatic interaction

$$-\sum_i\int n_{\rm oh}(\vec{r}-\vec{R}_i)\delta V_{\rm struc}(\vec{r}-\vec{R}_i)d\vec{r}\ . \tag{35}$$

This replaces the relatively complicated series of terms generated in the formalism of paper I [e.g., Eqs. (66) and (67)]. Furthermore, since $\delta V_{\rm struc}$ itself can be expressed in terms of fundamental quantities, via Eq. (14), the additional contribution (35) may be readily absorbed into the existing framework of the theory. The actual energy derivation which accomplishes this task parallels that given in paper I and is also briefly discussed in Appendix A. We concentrate here only on the new forms that our characteristic functions assume in the optimized GPT and the relationship of these results to the ones obtained in paper I.

The three major components of the total electron

density are still defined by Eq. (2), with $\delta n_{\rm val}(q)$ now divided into orthogonalization-hole and screening terms according to Eqs. (21)–(28). The new orthogonalization-hole quantities may be directly calculated from these equations, while comparably explicit formulas for the screening density $n_{\rm scr}(q)$ are obtained from Eq. (27) above and Eqs. (47)–(54) of paper I:

$$n_{\rm scr}(q)=\frac{4}{(2\pi)^3}\left[\int_{k<k_F}\frac{w_0(\vec{k},\vec{q})}{\epsilon_{\vec{k}}-\epsilon_{\vec{k}+\vec{q}}}d\vec{k}\mp\int_{k\gtrless k_F}\frac{h_1(\vec{k},\vec{q})}{\epsilon_{\vec{k}}-\epsilon_{\vec{k}+\vec{q}}}d\vec{k}\right], \tag{36}$$

where

$$w_0(\vec{k},\vec{q})\equiv\langle\vec{k}+\vec{q}\,|\,w_0\,|\,\vec{k}\rangle$$
$$=v(q)+\sum_{\alpha=c,d}(\epsilon_{\vec{k}}-E_\alpha^{\rm vol})\langle\vec{k}+\vec{q}\,|\,\phi_\alpha\rangle\langle\phi_\alpha\,|\,\vec{k}\rangle+\sum_d(\langle\vec{k}+\vec{q}\,|\,\Delta_{\rm vol}\,|\,\phi_d\rangle\langle\phi_d\,|\,\vec{k}\rangle+\text{c.c.}), \tag{37}$$

with

$$v(q)=v_{\rm ion}(q)+\frac{4\pi e^2}{q^2}[1-G(q)][n_{\rm oh}(q)+n_{\rm scr}(q)], \tag{38}$$

and where

$$h_1(\vec{k},\vec{q})=\sum_d\frac{\langle\vec{k}+\vec{q}\,|\,\Delta_{\rm vol}\,|\,\phi_d\rangle\langle\phi_d\,|\,\Delta_{\rm vol}\,|\,\vec{k}\rangle}{\epsilon_{\vec{k}}-E_d^{\rm vol}}. \tag{39}$$

In the usual way, Eqs. (36) and (38) represent simultaneous coupled equations for $n_{\rm scr}(q)$ and $v(q)$ and may be combined to eliminate $v(q)$ and find $n_{\rm scr}(q)$. As above, one has quite generally the replacements

$$\langle\vec{k}\,|\,\Delta_{\rm pa}\,|\,\phi_d\rangle\rightarrow\langle\vec{k}\,|\,\Delta_{\rm vol}\,|\,\phi_d\rangle \tag{40}$$

and

$$E_d^{\rm pa}\rightarrow E_d^{\rm vol} \tag{41}$$

in all hybridization terms translated from the results of paper I. This remains true throughout the optimized GPT formalism. The actual quantitative effect of these latter replacements is, however, quite small and by themselves would not be especially significant.

To discuss the total energy as given by Eq. (3), we first separate out the very large but uninteresting core energy (per atom) $E_{\rm core}$ from the valence binding energy (per atom) $E_{\rm bind}$:

$$E_{\rm tot}=N(E_{\rm bind}+E_{\rm core}). \tag{42}$$

The valence binding energy in turn can be divided into a large volume contribution $E_{\rm vol}$ and a much smaller structure-dependent contribution $E_{\rm struc}$:

$$E_{\rm bind}=E_{\rm vol}+E_{\rm struc}. \tag{43}$$

We define $E_{\rm struc}$ to include the final two terms in Eq. (2) plus the structural component of the electrostatic energy,

$$E_{\rm es}^{\rm struc}=N^{-1}E_{\rm es}(Z^*)+\tfrac{9}{10}(Z^*e)^2/R_{\rm WS}. \tag{44}$$

Thus

$$E_{\rm struc}=E_{\rm es}^{\rm struc}+\sum_{\vec{q}}{}'\,|S(\vec{q})|^2F(q)$$
$$+\tfrac{1}{2}\sum_i{}'v_{\rm ol}(R_i), \tag{45}$$

where the prime on the final sum now excludes the $R_i=0$ term. Note that the definitions (42)–(45) imply the further relationship

$$E_0=N[E_{\rm vol}+E_{\rm core}+\tfrac{9}{10}(Z^*e)^2/R_{\rm WS}] \tag{46}$$

for the energy constant in Eq. (2).

The volume-dependent energy $E_{\rm vol}$ has the general form given by Eq. (69) of paper I (Ref. 19),

$$E_{\rm vol}=E_{\rm fe}+E_{\rm oh}+\frac{2\Omega_0}{(2\pi)^3}\left[\int_{k<k_F}w_0^{\rm pa}(\vec{k},0)[1+p(\vec{k})]d\vec{k}\right.$$
$$\left.\mp\int_{k\gtrless k_F}h_1(\vec{k},0)\left[1+p(\vec{k})-\frac{w_0^{\rm pa}(\vec{k},0)+h_1(\vec{k},0)}{\epsilon_{\vec{k}}-E_d^{\rm vol}}\right]d\vec{k}\right], \tag{47}$$

where $p(\vec{k})\equiv\langle\vec{k}\,|\,p\,|\,\vec{k}\rangle$ and $E_{\rm fe}$ is the free-electron binding energy

$$E_{\rm fe}=\tfrac{3}{5}Z\epsilon_F+Z\epsilon_{\rm xc}(n_{\rm unif})-\tfrac{3}{5}(Ze)^2/R_{\rm WS}\ , \tag{48}$$

from Eq. (77) of paper I. As in paper I, $w_0^{\rm pa}(\vec{k},0)$ is defined as the $q=0$ limit of $w_0(\vec{k},\vec{q})$ with the full potential v replaced by the zero-order pseudoatom potential

$$v_{\rm pa}=v_{\rm unif}+v_{\rm ion}\ . \tag{49}$$

The quantity $E_{\rm oh}$ in Eq. (47) is a small self-energy correction which takes account of the finite size of the orthogonalization hole:

$$E_{\rm oh}=-\frac{9}{10}\frac{(Z^*-Z)^2e^2}{R_{\rm WS}}+\tfrac{1}{2}\int_0^\infty u_{\rm oh}(r)\left[v_{\rm oh}(r)-\frac{(Z^*-Z)e^2r^2}{R_{\rm WS}^3}\right]dr\ , \tag{50}$$

where $u_{\rm oh}(r)=4\pi r^2 n_{\rm oh}(r)$ and $v_{\rm oh}$ is the direct Coulomb potential arising from $n_{\rm oh}$. Equation (50) replaces Eq. (62) of paper I.

The new energy-wave-number characteristic F and overlap potential $v_{\rm vol}$ now revert to more symmetrical and compact forms in which there is no explicit appearance of extra terms arising from the structure-dependence of the hybridization:

$$F(q)=\frac{2\Omega_0}{(2\pi)^3}\left[\int_{k<k_F}\frac{[w_0(\vec{k},\vec{q})]^2}{\epsilon_{\vec{k}}-\epsilon_{\vec{k}+\vec{q}}}d\vec{k}\mp\int_{k\gtrless k_F}\frac{2h_1(\vec{k},\vec{q})w_0(\vec{k},\vec{q})+[h_1(\vec{k},\vec{q})]^2}{\epsilon_{\vec{k}}-\epsilon_{\vec{k}+\vec{q}}}d\vec{k}\right]$$
$$-\frac{2\pi e^2\Omega_0}{q^2}\{G(q)[n_{\rm oh}(q)]^2+[1-G(q)][n_{\rm scr}(q)]^2\} \tag{51}$$

in place of Eq. (70) of paper I and

$$v_{\rm ol}(\,|\vec{R}_i-\vec{R}_j|\,)=\sum_d\left\{4S_d^{ij}\Delta_d^{ji}\Theta(\epsilon_F-E_d^{\rm vol})\right.$$
$$-\frac{4\Omega_0}{(2\pi)^3}\left[\int_{k<k_F}\{S_d^{ij}[(\epsilon_{\vec{k}}-E_d^{\rm vol})h_3^{ji}(\vec{k})+2h_4^{ji}(\vec{k})]+\Delta_d^{ij}h_3^{ji}(\vec{k})\}d\vec{k}\right.$$
$$\left.\left.\mp\int_{k\gtrless k_F}\left[S_d^{ij}h_1^{ji}(\vec{k})+\frac{\Delta_d^{ij}[2h_4^{ji}(\vec{k})+h_1^{ji}(\vec{k})]}{\epsilon_{\vec{k}}-E_d^{\rm vol}}\right]d\vec{k}\right]\right\}$$
$$+(n_{\rm core}^i+2n_{\rm oh}^i)v_{\rm nuc\text{-}core}^j+n_{\rm oh}^i\left[v_{\rm oh}^j-\frac{(Z^*-Z)}{Z_a}v_{\rm nuc}^j\right] \tag{52}$$

in place of Eq. (71) of paper I, where we have maintained the shorthand notations

$$n^iv^j\equiv\int n(\vec{r}-\vec{R}_i)v(\vec{r}-\vec{R}_j)d\vec{r}\ ,$$

$$S_d^{ij}\equiv\langle\phi_d^i\,|\,\phi_d^j\rangle\ ,$$

and

$$\Delta_d^{ij}\equiv\langle\phi_d^i\,|\,\Delta\,|\,\phi_d^j\rangle\ ,$$

and where

$$h_1^{ji}(\vec{k})=\frac{\langle\phi_d^j\,|\,\Delta_{\rm vol}\,|\,\vec{k}\rangle\langle\vec{k}\,|\,\Delta_{\rm vol}\,|\,\phi_d^i\rangle}{\epsilon_{\vec{k}}-E_d^{\rm vol}}\ ,$$

$$h_3^{ji}(\vec{k})=\langle\phi_d^j\,|\,\vec{k}\rangle\langle\vec{k}\,|\,\phi_d^i\rangle\ ,$$

and

$$h_4^{ji}(\vec{k})=\langle\phi_d^j\,|\,\vec{k}\rangle\langle\vec{k}\,|\,\Delta_{\rm vol}\,|\,\phi_d^i\rangle\ .$$

Here ϕ_d^i and ϕ_d^j are d states centered on the sites i and j, respectively. We continue to handle the spe-

cial two-center matrix element Δ_d^{ji} by the procedure developed in paper I, namely as the integral

$$\Delta_d^{ji} = \int \phi_d^*(\vec{r}-\vec{R}_j)[v_{\rm loc}(|\vec{r}-\vec{R}_i|) - v_{\rm pa}(|\vec{r}-\vec{R}_j|)]\phi_d(\vec{r}-\vec{R}_i)d\vec{r} . \quad (53)$$

Here the accuracy of Eq. (53), whose $m=0$, 1, and 2 components are the direct analogs of the familiar tight-binding matrix elements $-dd\sigma$, $-dd\pi$, and $-dd\delta$, is further tested through band-structure calculations, as discussed in Sec. IV below.

It is interesting to note that our new total energy expressions, Eqs. (42)—(53), have the same forms they would had we simply ignored the structure dependence of the hybridization and retained our original definitions of the orthogonalization-hole and screening densities, i.e., $n_{\rm oh}^0$ and $n_{\rm scr}^0$, making only the replacements (40) and (41). In other words, one can view the entire effect of $\Delta_{\rm struc}$ as being achieved by the simple substitutions

$$n_{\rm oh}^0 \rightarrow n_{\rm oh} \quad (54)$$

and

$$n_{\rm scr}^0 \rightarrow n_{\rm scr} \quad (55)$$

in addition to Eqs. (40) and (41). This is a rather remarkable result and quite likely more general than the special cases of filled and empty d bands. We suspect, in fact, that the result is independent of the filling of the d bands and hence applicable to transition metals, although we do not as yet have an explicit proof of this supposition.

In addition to the formal simplicity of Eqs. (51) and (52), these expressions more closely reflect the relative importance of the structure dependence of the hybridization to calculated physical properties. In Fig. 3 we show the normalized energy-wave-number characteristic (with F in Ry a.u.)

$$F_N(q) = -(q^2\Omega_0/4\pi Z^{*2})F(q) \quad (56)$$

for Zn calculated from Eq. (51) and those obtained in paper I both with and without the effects of $\Delta_{\rm struc}$ included. The same comparison is made in Fig. 4 for the overlap potential of Zn. From these results, one can see that the apparent effect of $\Delta_{\rm struc}$ on the characteristic functions is much less in the present formalism than in the formalism of paper I, although clearly still significant. Of course, since the optimized GPT equations given above are, apart from the replacements (40) and (41), only a mathematical transformation of the results of paper I, almost the same calculated physical properties are obtained from either formalism.

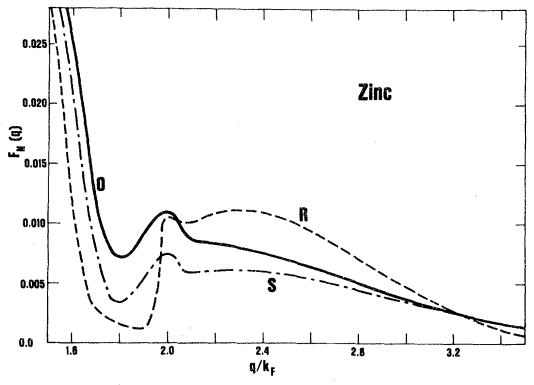

FIG. 3. Normalized energy-wave-number characteristic $F_N(q)$ for Zn as calculated from the present optimized theory via Eq. (51) (curve marked O) and from the formulation of paper I (Ref. 7) both with (curved marked R) and without (curve marked S) the structure dependence of the hybridization included.

This is shown in Tables II and III for Ca and Zn, respectively.

The range of physical properties considered in Tables II and III, as well as below, has been expanded over paper I to include full consideration

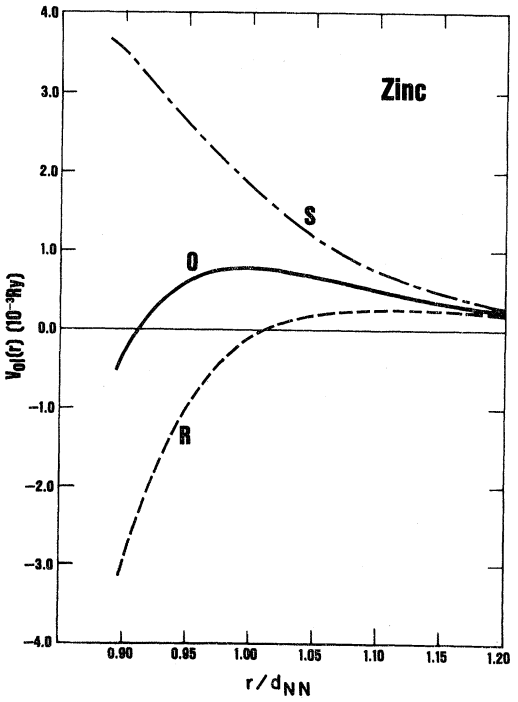

FIG. 4. Overlap potential $v_{\rm ol}(r)$ for Zn, where $d_{\rm NN}$ is the fcc nearest-neighbor distance and the notation is otherwise the same as Fig. 3.

TABLE II. Calculated properties of Ca with four different treatments of hybridization in the generalized pseudopotential theory (GPT). Quantities listed include the cohesive energy E_{coh} (Ry), equilibrium lattice constant a (a.u.), bulk modulus B (Mbar), resistivity of the liquid metal ρ_L ($\mu\Omega$ cm), fcc-bcc phase-transition temperature T_c (K), the fcc, bcc, and ideal hcp values of E_{struc} (Ry), Brillouin-zone-boundary phonon frequencies $\nu(q)$ (10^{12} Hz), and zero-point vibrational energy E^0_{ph} (Ry). Remaining energies are given in Ry.

	GPT[a]				Experiment	MJW[b]
Hybridization:	None	Paper I	Paper I	Present		
Volume	0	Δ_{pa}	Δ_{pa}	Δ_{vol}		
Structure	0	0	Δ'_{struc}	Δ_{struc}		
Band structure:[c]						
$X_{4'}-\Gamma_1$	0.36			0.36		0.34
$X_{4'}-X_1$	−0.01			0.07		0.09
$L_{2'}-\Gamma_1$	0.28			0.28		0.30
$L_{2'}-L_1$	−0.29			0.05		0.07
$E_F-\Gamma_1$	0.35			0.30		0.30
Cohesion:[c]						
E_{bind}	−1.430	−1.475	−1.478	−1.480	−1.458[d]	
E_{coh}	0.100	0.146	0.148	0.150	0.135[e]	0.165
a	11.0			10.7	10.6[f]	10.0
B	0.29			0.22	0.15[e]	0.17
Liquid Transport:						
ρ_L	9.8	31.5	31.5	31.5	23.0[g]	
Structural stability:						
$T=0$ phase	hcp (1.63)	fcc	fcc	fcc	fcc[f]	
high-T phase	bcc	bcc	bcc	bcc	bcc[f]	
T_c	195	660	590	582	721[h]	
$E^{bcc}_{struc}-E^{fcc}_{struc}$	0.000 34	0.001 67	0.001 75	0.001 69		
$E^{hcp}_{struc}-E^{fcc}_{struc}$	−0.000 31	0.000 80	0.000 90	0.000 91		
Lattice dynamics:[c]						
$\nu(q)$: L[100]	5.91	5.92	5.37	5.30		
T[100]	3.99	4.24	3.88	3.84		
L[111]	5.92	5.77	5.22	5.14		
T[111]	2.43	2.57	2.36	2.33		
E^0_{ph}	0.001 71	0.001 75	0.001 60	0.001 58	0.001 64[i]	

[a]All calculations, except of the lattice constant, refer to the observed density ($a=10.6$ and $\Omega_0=294.5$).
[b]Reference 18. All calculations refer to the computed equilibrium density ($a=10.0$ and $\Omega_0=251.4$) and the fcc structure.
[c]Calculated for the observed fcc structure.
[d]Reference 21.
[e]Reference 22.
[f]Reference 23.
[g]At the melting temperature of the metal from Ref. 24.
[h]Reference 25.
[i]Inferred from the observed Debye temperature $T_D=230$ K by the Debye formula $E^0_{ph}=\frac{9}{8}k_BT_D$.

of the band structure and cohesion. This allows us to now make a direct comparison with the density-functional calculations of MJW in addition to a comparison with experiment. We shall elaborate on these results in greater detail in Sec. IV. We wish only to emphasize here the very good overall description that the optimized GPT provides for the properties of Ca and Zn once a full treatment of the hybridization has been taken into account.

III. NOBLE METALS AND PARTIALLY FILLED d BANDS

We now turn our attention to the more challenging case of the noble metals. Originally, we con-

TABLE III. Calculated properties of Zn with four different treatments of hybridization in the generalized pseudopotential theory (GPT). Notation and units are the same as in Table II.

	GPT[a]				Experiment	MJW[b]
Hybridization	None	Paper I	Paper I	Present		
Volume	0	Δ_{pa}	Δ_{pa}	Δ_{vol}		
Structure	0	0	Δ'_{struc}	Δ_{struc}		
Band structure:[c,d]						
$X_{4'}-\Gamma_1$	0.68			0.68		0.72
$X_1-X_{4'}$	0.12			0.23		
X_5-X_1	0.0			0.11		0.12
$L_{2'}-\Gamma_1$	0.54			0.54		0.55
$L_1-L_{2'}$	0.03			0.13		0.16
$\Gamma_{25'}-\Gamma_1$	0.22			0.20		0.20
$E_F-\Gamma_1$	0.72			0.77		0.82
Cohesion:[c]						
E_{bind}	−2.144	−2.126	−2.136	−2.137	−2.111[e]	
E_{coh}	0.107	0.088	0.098	0.099	0.099[f]	0.129
a	7.36			7.46	7.43[g]	7.30
B	0.58			0.63	0.60[f]	0.82
Liquid Transport:						
ρ_L	18.3	38.9	38.9	41.2	37.4[h]	
Structural stability:						
Stable phase	hcp (1.64)	hcp (1.72)	hcp (1.94)	hcp (1.96)	hcp (1.86)[g]	
$E^{bcc}_{struc}-E^{fcc}_{struc}$	0.003 11	0.005 46	0.005 60	0.005 71		
$E^{hcp}_{struc}-E^{fcc}_{struc}$	−0.000 52	−0.000 95	−0.001 19	−0.001 28		
Lattice dynamics:[c]						
$\nu(q)$: L[100]	4.83	5.33	3.89	3.92		
T[100]	3.55	3.48	2.77	2.76		
L[111]	4.77	5.55	4.03	4.08		
T[111]	2.62	2.77	2.53	2.57		
E^0_{ph}	0.001 50	0.001 58	0.001 22	0.001 23		

[a]All calculations, except of the lattice constant, refer to the observed density ($a=7.43$ and $\Omega_0=102.7$).
[b]Reference 18. All calculations refer to the computed equilibrium density ($a=7.30$ and $\Omega_0=97.16$) and the fcc structure.
[c]Calculated for the fcc structure.
[d]In the quantities $X_1-X_{4'}$ and X_5-X_1, the upper and lower X_1 energies, respectively, are used.
[e]Reference 21.
[f]Reference 22.
[g]Reference 23. The c/a axial ratio is in parentheses.
[h]At the melting temperature of the metal from Ref. 26.

sidered these metals to represent the ideal testing ground for the filled-d-band limit of the GPT. Our initial applications,[1,3] in fact, were generally encouraging in this regard, although the calculated results were certainly not of the quality seen in Tables II and III. Nonetheless, we expected that subsequent refinements in both the theory and its implementation would greatly improve the situation. This has not proven to be the case. While such refinements have been steadily forthcoming[4,6,7] and have had a large positive impact on the application of the GPT to other metals, basic difficulties with the noble metals persist until one properly accounts for the unfilling of the d bands.

As suggested in Sec. II above, the inherent problems with a filled-d-band treatment of the noble metals are intimately related to the makeup of the electron density. The GPT implicitly demands

that the zero-order pseudoatom density,

$$n_{\rm pa}=n_{\rm unif}+n_{\rm core}\ , \tag{57}$$

represents a good first approximation to the actual electron density in one Wigner-Seitz cell of the metal, so that the first-order oscillatory density $\delta n_{\rm val}$ is indeed small. In actually constructing the pseudoatom, the uniform density is taken at its value in the metal,

$$n_{\rm unif}=Z/\Omega_0 \tag{58}$$

for $r<R_{\rm WS}$, and is set to zero (to preserve charge neutrality) for $r>R_{\rm WS}$. The core density,

$$n_{\rm core}(r)=\sum_{\alpha=c,d}\phi_\alpha^*(\vec{r})\phi_\alpha(\vec{r})\ , \tag{59}$$

where the sum is over occupied inner-core and d states, is then calculated self-consistently in the presence of $n_{\rm unif}$, using atomic boundary conditions on the inner-core states and applying the localization potential $v_{\rm loc}$ to the d states through the Schrödinger equation

$$(T+v_{\rm pa}+O_{\rm loc})\,|\,\phi_\alpha\rangle=E_\alpha^{\rm pa}\,|\,\phi_\alpha\rangle\ , \tag{60}$$

with

$$O_{\rm loc}=\begin{cases}0, & \alpha=c\\ v_{\rm loc}-\langle\phi_d\,|\,v_{\rm loc}\,|\,\phi_d\rangle, & \alpha=d\end{cases} \tag{61}$$

and

$$v_{\rm loc}(r)=\begin{cases}0, & r<R_{\rm WS}\\ V_0(r/R_{\rm WS}-1)^2, & r>R_{\rm WS}\ .\end{cases} \tag{62}$$

The r^2 dependence of $v_{\rm loc}$ as $r\to\infty$ gives the d states convenient Gaussian-type tails while the degree of localization is controlled by the single constant V_0. One may usefully think of V_0 as imposing an effective boundary condition on $\phi_d(\vec{r})$ at $r=R_{\rm WS}$. As $V_0\to\infty$, the anti-bonding-like condition

$$\phi_d(R_{\rm WS})=0 \tag{63}$$

is obtained, while as $V_0\to 0$ the bondinglike condition

$$\frac{\partial\phi_d(R_{\rm WS})}{\partial r}=0 \tag{64}$$

is approached (although never actually reached in practice). The intermediate Andersen condition[27]

$$\frac{R_{\rm WS}}{\phi_d(R_{\rm WS})}\frac{\partial\phi_d(R_{\rm WS})}{\partial r}=-3 \tag{65}$$

gives a d state corresponding to the approximate center of the d band and can be obtained by iterating V_0.

The arbitrariness in $v_{\rm loc}$ and V_0 simply reflect the arbitrariness in selecting a basis state, in this case ϕ_d. As we have discussed previously,[6,7] there is a built-in insensitivity in the GPT to the choice of V_0 over wide ranges of values. In practice, one seeks optimization and the following criteria represent the practical requirements of a suitable range:

(i) The d states ϕ_d must be localized to the degree that the effective strength of the hybridization potential Δ is minimized or at least weak, as measured by the matrix elements $\langle\vec{k}\,|\,\Delta_{\rm vol}\,|\,\phi_d\rangle$ and Δ_d^{ij} and the requirement

$$\Delta_{\rm vol}\gg\Delta_{\rm struc}\ . \tag{66}$$

This necessitates a substantial value of V_0, normally $V_0>10$ Ry.[6,7]

(ii) The zero-order pseudoatom electron density must be adequate to produce a good overall band structure for the metal. In particular, the position and width of the d band must be correctly established. A simple and direct test of this can be made through the logarithmic derivatives $D_l(E)$ associated with the pseudoatom potential $v_{\rm pa}$, which can be readily compared against those of a self-consistent band-structure potential. The critical points of comparison are the top of the d band (the X_5 level in the fcc structure), as marked by the antibonding condition

$$D_2(X_5)=-\infty\ , \tag{67}$$

and the bottom of the d band (the X_3 level in the fcc structure), as given by the bonding condition

$$D_2(X_3)=0\ , \tag{68}$$

where the logarithmic derivatives are evaluated at $r=R_{\rm WS}$.

(iii) For filled (or partially filled) d bands, the d basis states ϕ_d should actually correspond to the d band in the tight-binding sense. That is, the energy $E_d^{\rm pa}$ should mark the center of the d band, so that condition (65) is approximately satisfied, and the Δ_d^{ij} should correctly describe the structure of the d band.

For ideal applications (e.g., Ca and Zn) a substantial range of V_0 will work with (i) being the most important of the above criteria to be satisfied. In the case of empty-d-band metals, $v_{\rm pa}$ is independent of ϕ_d and hence V_0, so that criterion (ii) is an insensitive test, while criterion (iii) is of no important concern. For filled-d-band metals, ϕ_d is na-

turally well localized, so that not only is v_{pa} weakly dependent on V_0 but the d band is also very narrow. Consequently, neither (ii) nor (iii) are discriminating tests. Our now considerable experience with such cases[4,6,7] has led to the universal prescription

$$V_0=\begin{cases}\infty, & \text{empty-}d\text{-band metals}\\ 25\text{ Ry}, & \text{full-}d\text{-band metals}\end{cases}, \tag{69}$$

and, except for the noble metals, these values have been maintained throughout this paper.

This ideal situation is to be strongly contrasted with that in the noble metals. If one insists on keeping the d states completely occupied, so that $Z=1$, then it is impossible to simultaneously satisfy all three of the above criteria. This can be seen from Fig. 5, where we have plotted (dashed lines) the top (X_5) and width (X_5-X_3) of the d band in Cu vs V_0, as determined by Eqs. (67) and (68), and compared the results against the values calculated from a self-consistent band-structure potential,[28] as obtained by the linear-muffin-tin-orbitals (LMTO) method.[27] One sees that although our calculated position and width of the d band vary slowly (approximately logarithmically) with V_0, they only asymptotically approach the band-structure results as $V_0\to 0$, remaining too large for $V_0>0$. On the other hand, criterion (iii), as measured by Eq. (65), is satisfied for $V_0=5.4$ Ry, while criterion (i) requires $V_0>10$ Ry. Thus a good electron density

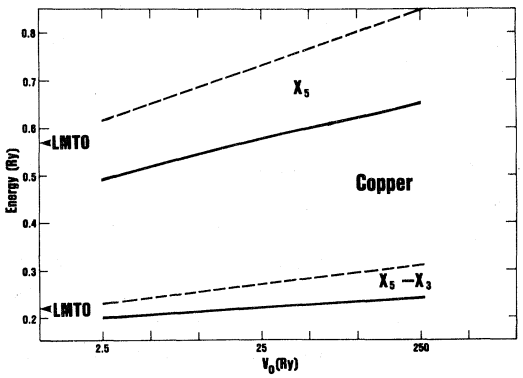

FIG. 5. Top (X_5) and width (X_5-X_3) of the d band in Cu vs localization potential parameter V_0 in Eq. (62), as determined from logarithmic derivatives of the zero-order pseudoatom potential v_{pa} via Eqs. (67) and (68). Dashed lines refer to a pseudoatom with filled d states and a valence $Z=1$, while solid lines refer to a pseudoatom with partially-filled d states and a self-consistent valence. Shown for comparison are the corresponding self-consistent linear-muffin-tin-orbital (LMTO) values of Ref. 28.

and band structure in the noble metals necessitates a spatially delocalized d state ($V_0\sim 0$), while a weak hybridization potential demands a highly localized d state ($V_0>10$ Ry). This basic difficulty cannot be overcome through any modification in the form of the localization potential v_{loc} and is, in fact, only resolved when the d states are allowed to unfill.

We have extended our zero-order pseudoatom method to permit partially occupied d states and a self-consistent valence Z. The additional equations governing the self-consistency follow quite naturally from the general formalism set forth in Ref. 2 and are essentially the relations describing the interaction of a bare ion placed in a free-electron gas. The number of d electrons Z_d retained by the ion is given by the phase-shift condition[29]

$$\begin{aligned}Z_d&=\frac{10}{\pi}\delta_2(\epsilon_F)\\&=\frac{10}{\pi}\tan^{-1}\left[\frac{-\mathrm{Im}\Gamma_{dd}(\epsilon_F)}{E_d^{\mathrm{vol}}+\mathrm{Re}\Gamma_{dd}(\epsilon_F)-\epsilon_F}\right],\end{aligned} \tag{70}$$

where $\Gamma_{dd}(E)$ is the so-called d-state self-energy[2] and the Fermi level ϵ_F is determined by the free-electron formula

$$\epsilon_F=\frac{\hbar^2}{2m}\left[\frac{3\pi^2 Z}{\Omega_0}\right]^{2/3}. \tag{71}$$

Additionally, Z and Z_d are constrained by the conservation of electrons condition

$$Z+Z_d=Z_a-Z_c \tag{72}$$

where Z_c is the number of inner-core electrons per ion. The self-energy $\Gamma_{dd}(E)$ can be directly expressed in terms of d-state hybridization quantities. Specifically,

$$\Gamma_{dd}(E)=-\frac{1}{\pi}\mathscr{P}\int_0^\infty \frac{f(\epsilon_{\vec{k}},E)}{\epsilon_{\vec{k}}-E}d\epsilon_{\vec{k}}-if(E,E), \tag{73}$$

where $\mathscr{P}$ denotes principal value and

$$f(\epsilon_{\vec{k}},E)=\Omega_0 k[(E-E_d^{\mathrm{vol}})\beta(k)+\Delta_{\mathrm{vol}}(k)]^2, \tag{74}$$

with

$$\langle\vec{k}\,|\,\Delta_{\mathrm{vol}}\,|\,\phi_d\rangle=-4\pi\Delta_{\mathrm{vol}}(k)Y_{2m}(\vec{k}) \tag{75}$$

and

$$\langle\vec{k}\,|\,\phi_d\rangle=-4\pi\beta(k)Y_{2m}(\vec{k}). \tag{76}$$

Here $Y_{2m}(\vec{k})$ is the usual $l=2$ spherical harmonic. Equations (70)—(72) then represent three simultaneous equations in three unknowns: Z, Z_d, and ϵ_F. For a full self-consistent treatment, these equations must be iterated to solution in conjunction with the defining Eqs. (57)—(62) of the pseudoatom.

We have calculated such self-consistent pseudoatoms for Cu as a function of V_0. The new self-consistent valence Z so obtained varies little with V_0 but remains significantly greater than one in all cases: $1.66 \leq Z \leq 1.78$ for $2.5 \leq V_0 \leq 250$ Ry. More importantly, the large redistribution of electrons accompanying the unfilling of the d states leads to just the lowering of band energies needed to satisfy all three excellence criteria stated above, as can be seen in Fig. 5. In particular, the position and width of the d band now match the LMTO values for sufficiently large V_0 to satisfy both criteria (i) and (iii). The Andersen boundary condition (65) is met, in fact, for $Z=1.66$ and $V_0=14.6$ Ry and adequately represents the desired condition of optimization. We have tested the sensitivity of these results by repeating the pseudoatom calculations in Cu under pressure (i.e., at smaller atomic volumes), where corresponding LMTO logarithmic-derivative data was available to us,[28] maintaining Eq. (65) in each case. A comparison of resulting LMTO and pseudoatom band energies at several different densities is made in Fig. 6, where we have also included calculated values for the bottom of the p band (the $L_{2'}$ level in the fcc structure), as determined by

$$D_l(L_{2'})=0 \,. \tag{77}$$

The agreement is clearly excellent in every respect, confirming the significance of our approach.

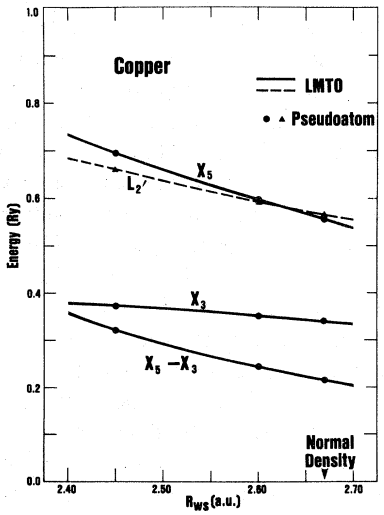

FIG. 6. Band energies in Cu under compression as determined from the logarithmic derivatives of self-consistent pseudoatom [Eqs. (57)—(62), (65), and (70)—(72)] and LMTO (Ref. 28) potentials via Eqs. (67), (68), and (77).

We are now in the process of extending the full optimized GPT of Sec. II to partially-filled-d-band metals. This work will be reported in later papers, but one available result is of direct interest to the present discussion, namely the magnitude of the oscillatory density $\delta n_{\rm val}$. As required by the formal structure of the theory, this quantity is indeed found to be small when a self-consistent valence is used as the basis for the calculation. This is shown in Table IV, where approximate values for the componenets of the total electron density, Eq. (2), are given at the midpoint between nearest neighbors in Cu. For comparison, corresponding values obtained from a comparable filled-d-band description of Cu are also listed.

We have further calculated zero-order pseudoatoms across the $3d$ transition series from Ca to Zn. The self-consistent valences so obtained are plotted in Fig. 7, where it is seen that Z remains relatively constant ($Z \sim 1.5$) until one reaches Zn, with both Ca and Cu appearing as natural members of the transition metals. With respect to our present concern, the crucial factor which separates Ca from Cu is the different quantitative relationship between the self-consistent and nominal free-atom values of Z in the two cases. For Ca, the former valence is 1.59 while the latter is 2, so that maintaining an empty-d-band description of the metal implies a maximum first-order elec-

TABLE IV. Approximate components of the normalized electron density, $\Omega_0 n$, at the midpoint between nearest neighbors in fcc Cu as calculated from a filled-d-band treatment of the metal and from a partially-filled-d-band treatment with a self-consistent valence. In both cases, the basis d states satisfy the Andersen boundary condition (65).

	Filled d band ($V_0=5.4$ Ry)	Paritally-filled d band ($V_0=14.6$ Ry)
$\Omega_0 n_{\rm unif}$[a]	1.00	1.66
$2\Omega_0 n_{\rm core}$	1.66	1.26
$\Omega_0 \delta n_{\rm val}$[b]	0.86	0.19
$\Omega_0 n$	3.52	3.11

[a]Note $\Omega_0 n_{\rm unif}=Z$.

[b]Calculated as $\delta n_{\rm val}=(Z^*-Z)/\Omega_0+2n_{\rm oh}+\langle n_{\rm scr}\rangle$, where $\langle n_{\rm scr}\rangle$ is a spherical average of Eq. (26).

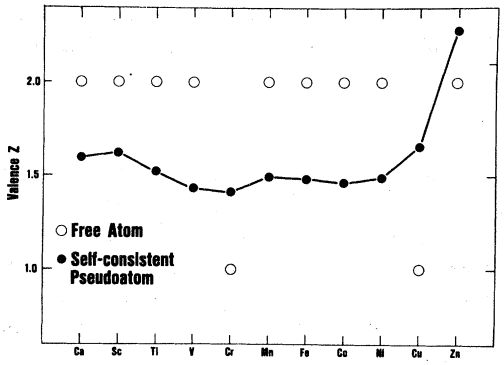

FIG. 7. Self-consistent valence across the $3d$ transition series as obtained from the pseudoatom defined by Eqs. (57)–(62), (65), and (70)–(72). Shown for comparison is the nominal free-atom valence.

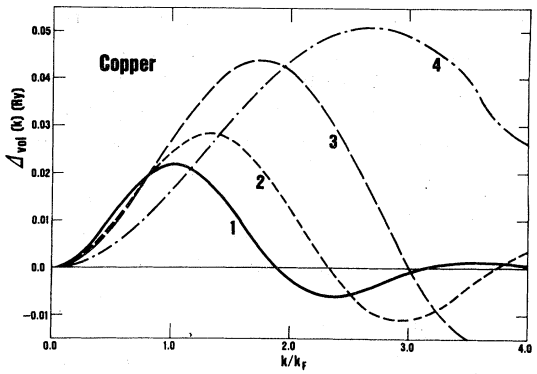

FIG. 8. Hybridization integral $\Delta_{vol}(k)$ in Cu for $Z=1$ under various conditions of d-state localization. Curves 1, 2, and 3, respectively, refer to $V_0=5.4$, 100, and ∞ Ry in Eq. (62). Curve 4 is the corresponding result of Dagens (Ref. 15).

tron density perturbation of $\sim 20\%$. For Cu, on the other hand, one has $Z=1.66$ self-consistently versus $Z=1$ for a filled-d-band description, a much larger 66% perturbation. Finally in Zn, the self-consistent valence is 2.28 as compared to a free-atom value of 2, only a $\sim 15\%$ perturbation. Thus our self-consistent valence description of the metal confirms the adequacy of the empty- and filled-d-band treatments of Ca and Zn, respectively, while separating out Cu for special treatment.

To complete the argument, we should comment on the recent work of Dagens and co-workers,[13–17] which suggests, on the surface at least, a different conclusion. Dagens's resonant-model-potential (RMP) scheme is the first serious attempt to develop a model potential analog to the GPT and the success of the full-d-band limit of the RMP in calculating such things as phonon frequencies and structural energies in the noble metals is both noteworthy and surprising in light of the above discussion. Our purpose here is not a detailed comparison between the GPT and RMP schemes, which, in any case, would be difficult due to the vastly different details of the two methods, but we can offer a tentative explanation of the apparent paradox. The success of Dagens's full-d-band treatment of the noble metals, we believe, stems from the fact that the RMP scheme is ultimately a parametrization which relaxes certain inherent theoretical constraints, in particular, the constraints among the spatial extent of the d states, the electron density, and the form of the hybridization integral $\Delta_{vol}(k)$. Dagens begins with an arbitrarily chosen form for $\Delta_{vol}(k)$, namely

$$\Delta_{vol}(k)=\left[\frac{A_d}{4\pi}\right]^{1/2}\frac{k_0^2}{k_0^2-k^2}j_2(kR_M)\ ,$$

where A_d and R_M are parameters and k_0R_M is the first nonvanishing zero of the $l=2$ spherical Bessel function j_2. He maintains a nonoverlapping representation (i.e., $v_{ol}=0$) by constraining the model radius R_M to be less than half of the nearest-neighbor distance in the metal. In the GPT this corresponds to an ultralocalized d state ϕ_d of approximately the same spatial extent. Localizing ϕ_d has the effect of pushing out $\Delta_{vol}(k)$ in $\vec{k}$ space, as shown in Fig. 8, so that Dagens's hybridization integral is much more extended than even that arising from the $V_0\rightarrow\infty$ limit of our scheme. In the context of our previous discussion surrounding Eq. (34), this explains Dagens's relatively large calculated values of Z^* for the noble metals, since an integral of $\Delta_{vol}(k)$ over $k>k_F$ is involved. At the same time, of course, it creates the theoretical dilemma of a very poor zero-order electron density and a large δn_{val}, as we have discussed. Dagens's scheme effectively sidesteps this difficulty by not separating zero- and first-order components of the electron density in determining his remaining parameters (e.g., A_d). Instead, he requires only that angular components of the *total* electron density be constrained through the matching of appropriate logarithmic derivatives to an external calculation of the same in the interstitial region surrounding each ion. To obtain the latter, he introduces a so-called Wigner-Seitz neutral atom[15] (similar to our zero-order pseudoatom) with a d component of electron density established not by an antibonding condition like (63) [or $\phi_d(R_M)=0$, which would be consistent with his Δ_{vol}], but rather by the bonding condition (64). As we have seen above, this procedure does indeed produce a good electron density with $Z=1$, although clearly such a

construction has no self-consistent link to the RMP theory itself. Nonetheless, RMP parameters so determined are expected to yield the correct interstitial density and this in turn appears to be instrumental in Dagens's success.

In the context of the optimized GPT, it is also possible to obtain a workable, although less reliable, filled-d-band description of the noble metals through *ad hoc* adjustment in the formalism of Sec. II. This can be done via the following recipe:

(i) In the spirit of Dagens, choose a highly localized d-state representation ($V_0 \gg 10$ Ry) and drop $v_{\rm ol}$;

(ii) Compensate for the fact that $E_d^{\rm pa}$ (and also the core levels $E_c^{\rm pa}$) then lie way too high in energy by adding to $E_\alpha^{\rm pa}$ a large negative core shift $E_{\rm cs}$;

(iii) Treat $E_{\rm cs}$ as an adjustable parameter to obtain the best overall description of the metal.

For illustrative purposes, we have adopted here such a scheme with $V_0 = 100$ Ry and $E_{\rm cs} = -0.4317$, -0.3293, and -0.4035 Ry in Cu, Ag, and Au, respectively. This scheme was used to obtain the noble-metal results listed in Table I and is also applied to the calculation of physical properties in Sec. IV below. With regard to the latter, the level of achievement of our original work on the noble metals[1,3] is approximately recovered. It is entirely possible that a more successful recipe could be found, *vis-á-vis* that of Dagens, but we have not pursued this since it seems clear at this point that any filled-d-band treatment of the noble metals is at best a stopgap measure.

IV. APPLICATIONS

We summarize in this section extensive calculations that we have made on the properties of the 22 nontransition metals. Except in the case of the noble metals, these results represent an unaltered application of the optimized GPT described in Sec. II, with the only external input to the calculations being the atomic number Z_a, the valence Z, and (for convenience) the atomic volume Ω_0. As in paper I and above, we treat the heavy alkali and alkaline-earth metals in the empty-d-band limit of the theory, the group-IIB metals in the filled-d-band limit and the remaining metals in the simple-metal limit.[30] For the noble metals, we present results obtained from the *ad hoc* filled-d-band scheme introduced in Sec. III and, in the case of Cu, our currently available results from the partially-filled-d-band extension of the optimized GPT, also discussed in Sec. III.

A. Band structure

We have shown above that certain critical features of the band structure can be estimated from the logarithmic derivatives associated with the zero-order pseudoatom potential. A more complete (and slightly more accurate) description of the band structure can be obtained by setting up a full secular determinant of the hybrid nearly-free-electron tight-binding (H-NFE-TB) form. To do this, one begins with a pseudo-Hamiltonian matrix expressed in a plane-wave, localized-d-state representation. Following Pettifor,[31] one can then make a set of three exact transformations to effectively orthogonalize the basis functions and remove all energy dependence from the off-diagonal matrix elements. For the case of narrow d bands, one can also simplify the exact result by neglecting in each entry of the transformed matrix all terms higher than first-order in smallness. Then the secular determinant for the band structure $E(\vec{k})$ has the simple H-NFE-TB block structure

$$\begin{vmatrix} [\epsilon_{\vec{k}-\vec{G}} - E(\vec{k})]\delta_{\vec{G}\,\vec{G}'} + \langle \vec{k}-\vec{G} \mid w_0 \mid \vec{k}-\vec{G}' \rangle & -\langle \vec{k}-\vec{G} \mid \Delta_{\rm vol} \mid \phi_d \rangle \\ -\langle \phi_d \mid \Delta_{\rm vol} \mid \vec{k}-\vec{G}' \rangle & [E_d - E(\vec{k})]\delta_{dd'} - \sum_{j\neq 0} e^{i\vec{k}\cdot\vec{R}_j} \langle \phi_d^{i=0} \mid \Delta \mid \phi_{d'}^{j} \rangle \end{vmatrix} = 0 , \qquad (78)$$

where $\vec{G}$ and $\vec{G}'$ are reciprocal-lattice vectors. In this determinant five d states and all reciprocal-lattice vectors are spanned, but in practice only a small number of the latter are required to give a good description of states below the Fermi level.

For our purposes, the important feature of Eq. (78) is that the matrix elements which directly determine the band structure are a subset of those which govern the characteristic functions of the Sec. II. Thus comparing the predictions of Eq. (78) with the full local-density energy-band results of MJW gives us an independent check on the reliability with which we calculate these matrix elements and hence the characteristic functions them-

selves. This comparison is made in Table V. In obtaining our results in Table V, as well as Tables I and II above, we have employed the simplest possible analytic description of the states involved in each case. (The specific formulas used are given in Appendix B.) Bearing this in mind, the agreement between the GPT and MJW band energies is generally excellent. The most notable exceptions are the *ad hoc* filled-*d*-band results on the noble metals, where the *d* band has been pushed too low in energy in each case by the core shift chosen. Smaller core shifts would obviously do better for the band structure, but at the same time would worsen the description of other properties.

B. Electron density

Another interesting property for comparison with the calculations of MJW is the electron density. From our perspective, the most revealing place to test this quantity is in the interstitial regions between ions. In Table VI we list our values for the normalized total electron density, $\Omega_0 n$, and its components, evaluated at the midpoint between nearest neighbors in the 22 metals under consideration here. Also given in Table VI are MJW's calculated values of $\Omega_0 n$. In this case, the comparison is somewhat less precise than with other properties because of the spherical averaging (i.e., the muffin-tin approximation) inherent in the MJW calculations. Physically, one expects a local maximum in the electron density at the midpoint between nearest neighbors, so that the MJW values should represent an approximate lower bound at that point. This expectation is clearly borne out in Table VI, where one sees that our calculated results generally follow the trends of MJW but are larger in magnitude. Also evident from Table VI is the fact that our internal theoretical requirement

TABLE V. Selected band energies for 22 nontransition metals, as calculated from the generalized pseudopotential theory (GPT) and compared against the theoretical results of Moruzzi, Janak, and Williams (MJW, Ref. 18). The values listed refer to the bcc structure in the alkali metals and Ba and to the fcc structure otherwise. All energies are given in Ry.

Metal	$E_F-\Gamma_1$		$E_d-\Gamma_1$[a]		$L_{2'}-\Gamma_1$		$L_1-L_{2'}$[b]		$X_{4'}-\Gamma_1$		$X_1-X_{4'}$[b]		X_5-X_1	
	GPT	MJW	GPT	MJW	GPT	MJW	GPT	MJW	GPT	MJW	GPT	MJW	GPT	MJW
Li	0.30	0.26												
Na	0.24	0.26												
K	0.16	0.18	0.63											
Rb	0.15	0.16	0.59											
Cs	0.13		0.43											
Be	0.93	0.87			0.56	0.47	0.30	0.41	0.76	0.67	0.40			
Mg	0.52	0.52			0.39	0.39	0.02	0.04	0.50	0.51	0.08	0.06		
Ca	0.30	0.30	0.57		0.28	0.30	−0.05	−0.07	0.36	0.34	−0.07	−0.09		
Sr	0.27	0.26	0.61		0.26	0.29	−0.07	−0.10	0.33	0.28	−0.08	−0.08		
Ba	0.23		0.52											
Cu[c]	0.72	0.69	0.49	0.48	0.61	0.61	0.34	0.37[e]	0.80	0.81	0.39		0.26	0.27
Cu[d]	0.71	0.69	0.30	0.48	0.57	0.61	0.46	0.37[e]	0.77	0.81	0.52		0.31	0.27
Ag[d]	0.56	0.53	−0.03	0.18	0.48	0.50	0.36		0.65	0.66	0.43		0.29	0.26
Au[d]	0.63		−0.13		0.51		0.44		0.69		0.51		0.40	
Zn	0.77	0.80	0.21	0.21	0.54	0.55	0.13	0.16	0.68	0.72	0.23		0.11	0.12
Cd	0.64	0.63	−0.05	−0.08	0.44	0.44	0.11	0.11	0.58	0.56	0.21	0.18	0.11	0.11
Hg	0.65		−0.02		0.44		0.13		0.55		0.23		0.15	
Al	0.84	0.82			0.49	0.48	0.01	0.02	0.61	0.62	0.10	0.08		
Ga	0.81	0.84	−0.42	−0.31	0.50	0.52	−0.05	−0.04	0.60	0.64	0.07	0.04		
In	0.70	0.68	−0.49	−0.47	0.42	0.42	−0.00	−0.03	0.50	0.52	0.10	0.04		
Tl	0.68		−0.41		0.40		0.01		0.48		0.11			
Sn	0.80		−0.98		0.42		−0.06		0.49		0.06			
Pb	0.77		−0.80		0.40		−0.05		0.46		0.07			

[a]The MJW results refer to $E_d=\frac{3}{5}\Gamma_{25'}+\frac{2}{5}\Gamma_{12}$.

[b]L_1 and X_1 are the lower levels for Ca and Sr and the upper levels otherwise.

[c]Partially-filled-*d*-band GPT treatment with a self-consistent valence of $Z=1.66$.

[d]*Ad hoc* filled-*d*-band GPT treatment, as described in Sec. III of the text.

[e]J. F. Janak, A. R. Williams, and V. L. Moruzzi, Phys. Rev. B 6, 4367 (1972).

TABLE VI. Approximate components of the normalized total electron density, $\Omega_0 n$, at the midpoint between nearest neighbors in 22 nontransition metals, as calculated from the generalized pseudopotential theory (GPT) in the manner of Table IV. Band-structure values of $\Omega_0 n$ obtained from the work of Moruzzi, Janak, and Williams (MJW, Ref. 18) are shown for comparison. Results refer to the bcc structure for the alkali metals and Ba and to the fcc structure otherwise.

Metal	GPT				MJW
	$\Omega_0 n_{\text{unif}}$	$2\Omega_0 n_{\text{core}}$	$\Omega_0 \delta n_{\text{val}}$	$\Omega_0 n$	$\Omega_0 n$
Li	1.00	0.00	0.07	1.07	1.08
Na	1.00	0.03	0.07	1.09	1.11
K	1.00	0.10	0.09	1.19	1.20
Rb	1.00	0.15	0.10	1.25	1.23
Cs	1.00	0.26	0.10	1.36	
Be	2.00	0.00	0.14	2.15	2.03
Mg	2.00	0.01	0.15	2.16	2.12
Ca	2.00	0.08	0.11	2.19	2.16
Sr	2.00	0.15	0.18	2.33	2.26
Ba	2.00	0.55	0.09	2.64	
Cu[a]	1.66	1.26	0.19	3.11	2.73
Cu[b]	1.00	1.43	1.07	3.50	2.73
Ag[b]	1.00	1.92	0.91	3.83	2.88
Au[b]	1.00	2.78	1.10	4.88	
Zn	2.00	0.67	0.27	2.94	2.68
Cd	2.00	0.95	0.30	3.25	2.80
Hg	2.00	1.39	0.38	3.77	
Al	3.00	0.01	0.21	3.22	2.98
Ga	3.00	0.19	0.12	3.31	2.75
In	3.00	0.38	0.21	3.59	2.88
Tl	3.00	0.58	0.23	3.81	
Sn	4.00	0.15	0.22	4.37	
Pb	4.00	0.26	0.26	4.52	

[a]Partially-filled-*d*-band GPT treatment with a self-consistent valence of $Z=1.66$.
[b]*Ad hoc* filled-*d*-band GPT treament, as described in Sec. III of the text.

$$n_{\text{unif}} \gg \delta n_{\text{val}}$$

is well satisfied in all cases except the filled-*d*-band noble metals.

C. Cohesion

The calculation of the cohesive energy E_{coh} in the context of the GPT was discussed at length in Ref. 8. In that paper we reduced E_{coh} to a difference in the free-atom valence energy, $E_{\text{bind}}^{\text{atom}}$, and the corresponding metal binding energy plus zero-point vibrational energy, $E_{\text{bind}}+E_{\text{ph}}^{0}$:

$$E_{\text{coh}}=E_{\text{bind}}^{\text{atom}}-E_{\text{bind}}-E_{\text{ph}}^{0} . \tag{79}$$

The specific calculations of E_{bind} and E_{ph}^{0} in Ref. 8 were made on the basis of the characteristic functions of paper I. As shown in Tables I and II above, the effect of optimization on the former quantities is typically small, a few percent or less, so that the detailed analysis and comparison of E_{coh} with MJW made in Ref. 8 remains essentially intact and will not be repeated here. In the case of the noble metals, only first-order calculations of E_{bind} were considered previously. These have now been extended to normal second-order calculations within the framework of our *ad hoc* filled-*d*-band scheme. The net impact is only 10% or less in each case. All of our present calculated values of E_{coh} are summarized and compared with experiment in Fig. 9.

We have now extended our investigation of cohesion to include the volume dependence of E_{coh} in order to obtain both the equilibrium lattice constant and the bulk modulus. The former is determined in the usual way by requiring that the internal pressure,

$$P_i=\frac{\partial E_{\text{coh}}}{\partial \Omega_0} \tag{80}$$

vanish at equilibrium, while the latter is obtained

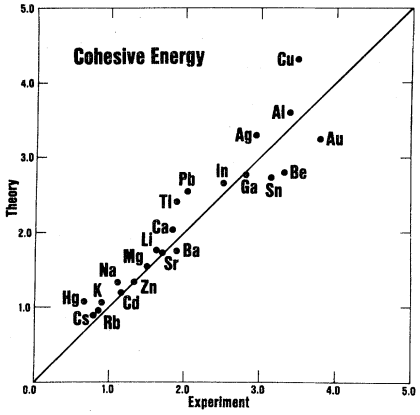

FIG. 9. Cohesive energy as calculated from the generalized pseudopotential theory (GPT) via Eq. (79) and compared against experiment (Ref. 22). Results for the noble metals were obtained from the *ad hoc* filled-*d*-band scheme discussed in Sec. III of the text. All values are given in eV.

by the method of homogeneous deformation through the defining relation

$$B=-\Omega_0\frac{\partial^2 E_{\rm coh}}{\partial\Omega_0^2} \tag{81}$$

In both cases we calculate $E_{\rm coh}$ on a suitable mesh and take the volume derivatives numerically. We have so far made actual calculations of the lattice constant and bulk modulus for only a few selected metals, but we expect that these results are representative. Values for the prototype empty-*d*-band metal Ca and the prototype filled-*d*-band metal Zn were given above in Tables I and II, respectively, and show reasonably good agreement with both MJW and experiment. The effect of hybridization on cohesion is seen to be quite important in Ca and smaller but still significant in Zn. Favorable results have also been obtained in the simple metals Be and Al, the only other cases tested to date.

D. Resistivity of the liquid metal

Electron transport properties for the metals under consideration here depend on the form factor

$$w(q)=w_0(\vec{k}_F,\vec{q})+h_1(\vec{k}_F,\vec{q})\ . \tag{82}$$

A simple calculation which offers some test of $w(q)$ is that of the liquid-metal resistivity by the well-known Ziman formula[9,32]

$$\rho_L=C\left[\frac{\Omega_0}{\epsilon_F^3}\right]\int_0^{2k_F}a(q)[w(q)]^2q^3dq\ , \tag{83}$$

where C is a constant and $a(q)=N\,|\,S(\vec{q})\,|^2$ is the so-called intensity function. Near the melting point of the metal, $a(q)$ is very nearly a universal function and for $q<2k_F$ can be calculated to a first approximation by the familiar liquid hard-sphere model with an assumed packing density of 0.45, as proposed by Ashcroft and Lekner (AL).[33] Using the AL intensity function and solid-density form factors and volumes, we have calculated ρ_L for the 22 nontransition metals. These results are displayed and compared with experiment in Fig. 10. Corrections for the true $a(q)$ function and liquid volume are both typically in the 10—15% range, so that the agreement for the lighter nonnoble metals is reasonable. The larger discrepancies for the heaviest metals (Au, Hg, Tl, and Pb) are possibly explained by our nonrelativistic treatment of these elements. However, similar discrepancies are also seen in Sr, Ba, and Cd. These may reflect to some extent a sensitivity of the calculated results to the hybridization potential.[4] Certainly, the effect of hybridization on ρ_L is quite large in both the heavy alkaline-earth metals (a factor of 3 to 6) and the group-II*B* metals (a factor of 2 to 3), as seen in Tables I and II.

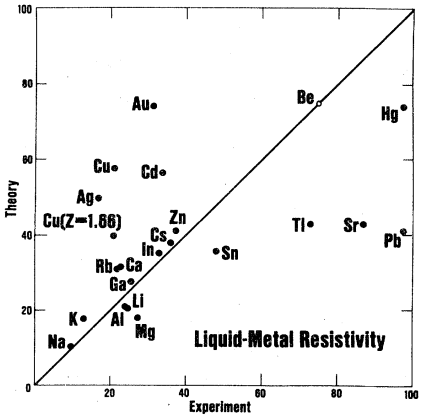

FIG. 10. Liquid-metal resistivity as calculated from the generalized pseudopotential theory (GPT) via Eq. (83) and compared against experiment (Refs. 24 and 26) at the melting temperature of the metal. The result marked Cu ($Z=1.66$) was obtained from the partially-filled-*d*-band extension of the GPT, while the remaining noble-metal results were obtained from the *ad hoc* filled-*d*-band scheme, as discussed in the text. An experimental resistivity has not been reported in the literature for Be. Also not shown are the calculated (154) and measured (338) resistivities in Ba. All values are given in $\mu\Omega$ cm.

In the noble metals, both the unfilling of the d band and the liquid volume effect are also important factors. We have calculated ρ_L for Cu on the basis of our partially-filled-d-band treatment of the metal, using a T-matrix generalization of Eq. (82) for the form factor. As shown in Fig. 10, this reduces the calculated resistivity by about one-third. A similar reduction is also expected in the noble metals by doing the calculation at the true liquid volume,[1] and clearly in Cu this is about what is needed to reconcile theory and experiment. It is of interest to point out that our present filled-d-band form factors for the noble metals are actually very similar to those of our original treatment,[1,3] and the much higher calculated values of ρ_L obtained here are due not only to the use of solid-density parameters but also to the intensity function employed. Our previous calculations of ρ_L in the nobler metals[1,3] used the experimental $a(q)$ of Wagner *et al.*,[34] which are substantially different than the AL function, especially for Cu. A number of more recent structure factor measurements on liquid Cu,[35] however, suggest the former data to be in error and the AL $a(q)$ to be approximately correct.

E. Phonon spectrum

The calculation of the phonon spectrum[3,9,10] directly tests the structural component of the total energy, E_{struc}, through the characteristic functions $F(q)$ and $v_{\text{ol}}(r)$. We have computed both fcc and bcc phonon frequencies $\nu(q)$ along the [100], [110], and [111] symmetry directions in all 22 of the metals under investigation here. Except for the noble and relativistic metals, our results generally display the observed canonical behavior and may be quantitatively judged by the values of $\nu(q)$ at the Brillouin-zone boundaries. These values are given in Table VII and are compared with experiment in the cases where data is available. The alkali metals Na, K, and Rb show expected good agreement but the frequencies for the other light simple metals, Li and Al, are 10—30% too large. In the latter cases, however, one can proportionally reduce the magnitudes of the calculated frequencies by modifying the choice of pseudopotential. This can be done most successfully in the case of Al, where a small core shift E_{cs} added to the E_α^{vol} in Eq. (37) will bring the overall calculated phonon spectrum into 3% agreement with experiment. The model-potential studies of Dagens, Rasolt, and Taylor[36] on selected simple metals suggest a possible physical significance to this core shift. These workers found, in the context of the density-functional formalism, that a model potential adjusted to reproduce ionic-potential phase shifts led to phonon frequencies that are also too large by 10—30% in Li and Al, but that a model potential adjusted to reproduce the nonlinear screening electron density of a single ion lowered the calculated frequencies and in the case of Al led to the same good agreement with experiment. The implication here is that the core shift is folding into the pseudopotential neglected higher-order nonlinear screening effects.

In the case of the noble metals, the calculated zone-boundary phonon frequencies from our *ad hoc* filled-d-band scheme are also reasonable, but the shapes of the spectra are not adequate, especially in Cu, as shown in Fig. 11. In fact, the present Cu phonon spectrum is quite similar to our original result[3] with experimentally unseen, Kohn-type anomalies in all the same places. (Compare Fig. 11 with Fig. 11 of Ref. 3.) These features are not present in the RMP calculation of Upadhyaya and Dagens,[16,17] who found generally good agreement with experiment in both Cu and Ag. We are hopeful that the partially-filled-d-band treatment of the noble metals will greatly improve the GPT situation, but the necessary characteristic functions $F(q)$ and $v_{\text{ol}}(r)$ are not as yet available to be tested.

In the heaviest simple metal Pb neither the magnitude nor the shape of the observed phonon spectra is well produced by our calculation. As seen in Table VII, the computed zone-boundary frequencies range from 8% to 55% too large. In additior the experimental phonon branches[47] have rather unique features which are not obtained in our cal-

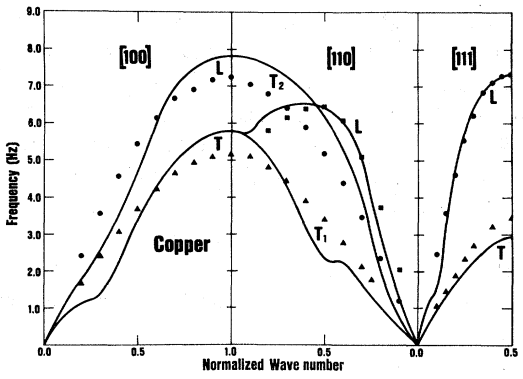

FIG. 11. Phonon spectrum for Cu as calculated from the *ad hoc* filled-d-band scheme of Sec. III of the text (solid lines) and compared against experiment (points; Ref. 42).

TABLE VII. Longitudinal (L) and transverse (T, T_1, and T_2) phonon frequencies at the Brillouin-zone boundaries in 22 nontransition metals, as calculated from the generalized pseudopotential theory (GPT) and compared against experiment. All values are in 10^{12} Hz.

Metal	GPT	Expt.	GPT	Expt.	GPT	Expt.	GPT	Expt.
bcc structure:	L[100]		L[110]		T_1[110]		T_2[110]	
Li	10.60	8.82[b]	11.87	9.00	2.18	1.90	6.30	5.70
Na	3.64	3.58[c]	3.82	3.82	0.85	0.93	2.57	2.56
K	2.17	2.21[d]	2.34	2.40	0.47	0.55	1.50	1.50
Rb	1.35	1.385[e]	1.49	1.50	0.27	0.34	0.92	0.96
Cs	1.04		1.19		0.21		0.68	
Ba	2.81		3.23		0.47		1.87	
fcc structure:	L[100]		T[100]		L[111]		T[111]	
Be	27.74		20.65		27.75		14.37	
Mg	8.02		5.68		7.99		3.82	
Ca	5.30		3.84		5.14		2.33	
Sr	3.48		2.43		3.41		1.48	
Cu[a]	7.82	7.25[f]	5.79	5.13	7.33	7.30	2.95	3.42
Ag[a]	4.41	4.95[g]	3.38	3.4	4.20	5.1	1.83	2.25
Au[a]	4.03	4.61[h]	2.83	2.75	3.94	4.70	1.49	1.86
Zn	4.46		3.15		4.59		2.78	
Cd	3.28		2.23		3.39		1.87	
Hg	2.55		1.70		2.65		1.45	
Al	10.74	9.67[i]	6.93	5.81	10.82	9.64	4.95	4.18
Ga	3.62		1.32		3.92		1.17	
In	3.51		1.69		3.68		1.20	
Tl	2.76		1.29		2.91		0.86	
Sn	2.79		1.48		3.51		1.14	
Pb	2.44	1.86[j]	1.38	0.89	2.95	2.185	0.96	0.89

[a] *Ad hoc* filled-*d*-band GPT treatment, as described in Sec. III of the text.
[b] At 98 K from Ref. 37.
[c] At 90 K from Ref. 38.
[d] At 9 K from Ref. 39; the T_1[110] frequency is at 4.3 K from Ref. 40.
[e] At 12 K from Ref. 41.
[f] At 49 K from Ref. 42.
[g] At 296 K, estimated from Fig. 1 of Ref. 43.
[h] At 296 K, from Ref. 44.
[i] Measured at 80 K by Ref. 45 and quoted from Table 2 of Ref. 46.
[j] At 100 K from Ref. 47.

culation, while at the same time certain anomalies are calculated which are not observed. This suggests to us that our nonrelativistic treatment is probably not adequate for describing the phonons in any of the heavy metals (Au, Hg, Tl, and Pb).

We have not as yet attempted to calculate phonon spectra for other lattice structures, but this would clearly be of interest in both the hcp metals (Be, Mg, Zn, and Cd) and the polyvalent metals with complex structures (Ga, In, and Sn), where ample experimental data is available for comparison.

F. Structural phase stability

An even more demanding test of the characteristic functions $F(q)$ and $v_{ol}(r)$ comes in the calculation of the relative energies of different crystal structures and the attempt to predict stable phases and phase transitions. The energy differences involved are indeed small: 10^{-5} to 10^{-3} Ry, but a clear and favorable pattern emerges if one is discriminating in one's application. To show this, let us first remove from consideration those metals for which trouble is expected *a priori*. These are (i) the heavy metals (Au, Hg, Tl, and Pb), because of neglected relativistic effects, (ii) metals with strong pseudopotentials and/or likely covalent effects (Li, Be, Ba, and Sn), because of neglected higher-order terms, and (iii) the remaining noble metals (Cu and Ag), because of the unreliability of our *ad hoc* filled-*d*-band scheme. This leaves 12 of our original 22 metals. Predictions of low- and high-temperature stable phases and phase-transition

temperature for these 12 metals are given in Table VIII and compared with experiment. The low temperature $T=0$ predictions are based on a comparison of the structural energies for fcc, bcc, sc (simple cubic), diamond, and hcp ($1.5 \leq c/a \leq 2.0$) structures at constant volume. Zero-point vibrational energies were determined to be negligible except in the alkali metals, but even there the results are not qualitatively altered. Extension of the calculation to finite temperature was made by considering the structural component of the total (electron plus phonon) Helmholtz free energy,

$$F_{\text{struc}} = E_{\text{struc}} + (k_B T/N) \times \sum_{\vec{q}} \ln\{2\sinh[h\nu(q)/2k_B T]\} , \quad (84)$$

and determining whether or not the bcc structure is stabilized at high temperature in the manner of Ref. 5.

The overall agreement with experiment exhibited in Table VIII is good, with the few qualitative errors easily explained. Consistent with experiment, we find that in all metals where a high-temperature transition to the bcc structure is not observed (Mg, Zn, Cd, Al, Ga, and In), the bcc structure is inherently unstable, as the entire $T_1[110]$ branch of the bcc phonon spectrum has imaginary frequencies. But in metals which *do* exhibit the bcc structure at some temperature (Na, K, Rb, Cs, Ca, and Sr), no such instabilities are found and reasonable transition temperatures T_c are also predicted. In that regard, our incorrect prediction of stable $T=0$ hcp structures for the heavy alkali metals can be viewed as a small quantitative error in the calculation of T_c. Indeed, had we done the calculations in these metals at slightly smaller atomic volumes, we would have found the observed bcc structure stable at $T=0$.[49] We furthermore find that for those metals exhibiting distorted structures (Zn, Cd, Ga, and In), the fcc structure is also unstable against distortion, with imaginary phonon frequencies occurring in the low-q modes of one or more of the transverse branches. In the cases of Zn and Cd, the structure dependence of the hybridization appears to account for the observed high c/a axial ratios, as shown in Table III. In Ga and In, the observed orthorhombic and tetragonal structures have not as yet been considered, but this would clearly be of interest.

Of the ten metals we have excluded from consideration in Table VIII, only for Li and Be are the correct $T=0$ structures obtained from a similar treatment. Both of these metals are hcp at low temperature, but the observed c/a axial ratios (1.64 in Li and 1.57 in Be) are not accurately predicted (1.61 in both Li and Be), and in Be there is some evidence[50] that the qualitative ordering of structur-

TABLE VIII. Predicted low- and high-temperature stable phases and transition temperature T_c (K) in 12 nontransition metals, as calculated from the generalized pseudopotential theory (GPT) and compared against experiment. For hcp phases the c/a axial ratio is given in parentheses.

	$T=0$ Phase		High-T Phase		T_c	
Metal	GPT	Expt.[a]	GPT	Expt.[a]	GPT	Expt.
Na	hcp (1.63)	hcp (1.63)	bcc	bcc	43	~36[b]
K	hcp (1.63)	bcc	bcc	bcc	33	none
Rb	hcp (1.63)	bcc	bcc	bcc	37	none
Cs	hcp (1.62)	bcc	bcc	bcc	25	none
Mg	hcp (1.63)	hcp (1.62)	hcp (1.63)	hcp (1.62)	none	none
Ca	fcc	fcc	bcc	bcc	582	721[c]
Sr	fcc	fcc	bcc	bcc	516	830[c]
Zn	hcp (1.96)	hcp (1.86)	hcp (1.96)	hcp (1.86)	none	none
Cd	hcp (1.88)	hcp (1.89)	hcp (1.88)	hcp (1.89)	none	none
Al	fcc	fcc	fcc	fcc	none	none
Ga[d]	sc	Ga-I	sc	Ga-I	none	none
In[e]	fcc	fct	fcc	fct	none	none

[a]Reference 23.
[b]Reference 48.
[c]Reference 25.
[d]The observed Ga-I structure is orthorhombic and was not considered in the GPT calculations.
[e]The observed fct structure is a tetrahedral distortion of the fcc structure and was not considered in the GPT calculations.

al energies is not correct either. In the case of the noble metals, the structural energies obtained with our *ad hoc* filled-*d*-band scheme show very similar behavior to those we found previously,[3] with distorted hcp structures favored to occur. Dagens,[14,15] on the other hand, has found the observed fcc structure to be stable in RMP calculations.

It is also instructive to consider the phase stability question as a function of pressure. In our original work on the alkaline-earth metals,[5] we calculated the slope of the bcc-fcc phase line, dT_c/dP, up to about 20 kbar in Ca and Sr. For both cases we found a positive slope in qualitative agreement with experiment[25] for Ca, although not for Sr. Optimized GPT calculations confirm the Ca result,[49] but Sr as yet has not been reinvestigated. In addition, both GPT and self-consistent LMTO calculations of the structural energy differences up to tenfold compression have very recently been made on the third-period simple metals Na, Mg, and Al.[51] The two methods show excellent qualitative agreement in their respective predictions as a function of pressure.

V. CONCLUSIONS

With the optimization of the GPT, we believe we have come close to realizing the full potential of generalized pseudopotential methods for empty- and filled-*d*-band metals. The optimized GPT not only adds simplicity, elegance, and computational efficiency to the density-functional formulation of the theory presented in paper I, but it has allowed us to discern more clearly the limitations of the empty- and filled-*d*-band treatments. The heavy alkaline-earth and group-II*B* metals have been confirmed to be ideal for applications in these limits. In Ca, Sr, Zn, and Cd, *d*-state hybridization effects are both important and accurately described by the optimized GPT set forth in Sec. II. In contrast, we have shown that rather severe difficulties occur in a filled-*d*-band treatment of the noble metals, with *ad hoc* adjustments required to provide even a marginal description of these materials.

Our optimized version of the GPT, of course, does not preclude the possibility of even further refinements and we fully expect these to occur in all limits of theory. For example, in the manner of Dagens, Rasolt, and Taylor,[36] it may well be possible to fold single-site, higher-order nonlinear screening effects into the pseudopotential and hybridization potential. At this point, however, we anticipate, as in the case of simple metals, that such refinements will be in the form of fine tuning of the optimized formalism we have developed here.

The more important priority at present is to fully develop the partially-filled-*d*-band extension of the GPT, which we briefly introduced in Sec. III. We have shown very clearly, in the case of Cu at least, that allowing the *d* states to unfill and a self-consistent valence to be achieved in zero-order provides an excellent starting point for the description of the metal. The development of corresponding characteristic functions has been accomplished for the electron density and is currently in progress for the total energy. This latter work will be reported in detail at a later time.

Note added in proof. Since the completion of this work, experimental phonon spectra in Ca have been reported by two separate groups: U. Buchenau, H. R. Schober, and R. Wagner, J. Phys. (Paris), Colloque C6, 395 (1981), and J. Zarestky, C. Stassis, B. N. Harmon, and R. M. Nicklow, Bull. Am. Phys. Soc. 27, 274 (1982). Both sets of measurements are in very good agreement with optimized GPT predictions, as will be discussed in a future publication. The former experimental zone-boundary frequencies for the $L[100]$, $T[100]$, $L[111]$, and $T[111]$ phonons in Tables II and VII are approximately 5.0, 3.7, 4.8, and 2.3, respectively.

ACKNOWLEDGMENTS

The author is grateful to Dr. A. K. McMahan for providing the LMTO results (Ref. 28) quoted in Sec. III of the text. Part of this work was performed under the auspices of the U. S. Department of Energy by Lawrence Livermore National Laboratory under Contract No. W-7405-Eng-48.

APPENDIX A

In this appendix we outline the modifications in the total energy derivation of paper I that lead to Eq. (35) and Eqs. (43)–(52) of the text. Our starting point is Eq. (21) of paper I for the total energy $E_{\rm tot}$. Dropping, as in paper I, the final group of negligible terms in that equation and further separating off the core energy as in Eq. (42) above, gives

$$NE_{\text{bind}}=n_{\text{unif}}\left[\tfrac{3}{5}\epsilon_F+\epsilon_{\text{xc}}(n_{\text{unif}})+\sum_i v^i_{\text{nuc-core}}\right]+\sum_\alpha \delta E_\alpha$$
$$+E_{\text{es}}(Z)-\tfrac{1}{2}\delta n_{\text{val}}\left[\delta V_{\text{val}}+\frac{d\mu_{\text{xc}}(n_{\text{unif}})}{dn}\delta n_{\text{val}}\right]+\tfrac{1}{2}{\sum_{i,j}}' n^i_{\text{core}} v^j_{\text{nuc-core}}\ , \tag{A1}$$

where we have used the definition (16) and the notation is otherwise the same as in paper I. The term $\sum_\alpha \delta E_\alpha$ includes first- and second-order band-structure contributions to E_{tot} and is of the form

$$\sum_\alpha \delta E_\alpha = N\frac{2\Omega_0}{(2\pi)^3}\left[\int_{k<k_F}(\langle \vec{k}\mid W_0-V\mid \vec{k}\rangle+\langle \vec{k}\mid W_0\mid \vec{k}\rangle\langle \vec{k}\mid \vec{P}\mid \vec{k}\rangle)d\vec{k}\right.$$
$$\left.\mp\int_{k\gtrless k_F}\sum_d \frac{\langle \vec{k}\mid \Delta\mid \phi_d\rangle\langle \phi_d\mid \Delta\mid \vec{k}\rangle}{(\epsilon_{\vec{k}}-E_d)}\left[1-\frac{\langle \vec{k}\mid W_0\mid \vec{k}\rangle}{(\epsilon_{\vec{k}}-E_d)}\right]d\vec{k}\right]+E_{\text{rest}}\ , \tag{A2}$$

where E_{rest} represents all additional second-order terms, which remain the same as in paper I except for the general replacements (40) and (41). The second-order contribution of the structure dependence of the hybridization to the total energy is contained entirely in the first-order components of Eq. (A2). The term involving $\langle \vec{k}\mid W_0-V\mid \vec{k}\rangle$ can be manipulated as in Eq. (60) of paper I to yield exactly

$$N\frac{2\Omega_0}{(2\pi)^3}\int_{k<k_F}\langle \vec{k}\mid W_0-V\mid \vec{k}\rangle d\vec{k}=N\frac{2\Omega_0}{(2\pi)^3}\int_{k<k_F} w_0^{\text{pa}}(\vec{k},0)d\vec{k}-n_{\text{unif}}\sum_i v^i_{\text{pa}}-\sum_i (n^0_{\text{oh}})^i\delta V^i_{\text{struc}}\ . \tag{A3}$$

The corresponding hybridization term can be analyzed by noting

$$\frac{\langle \vec{k}\mid \Delta\mid \phi_d\rangle\langle \phi_d\mid \Delta\mid \vec{k}\rangle}{\epsilon_{\vec{k}}-E_d}=\frac{\langle \vec{k}\mid (\Delta_{\text{vol}}+\Delta_{\text{struc}})\mid \phi_d\rangle\langle \phi_d\mid (\Delta_{\text{vol}}+\Delta_{\text{struc}})\mid \vec{k}\rangle}{\epsilon_{\vec{k}}-E_d^{\text{vol}}+\langle \phi_d\mid \delta V_{\text{struc}}\mid \phi_d\rangle}$$
$$=\frac{\langle \vec{k}\mid \Delta_{\text{vol}}\mid \phi_d\rangle\langle \phi_d\mid \Delta_{\text{vol}}\mid \vec{k}\rangle}{\epsilon_{\vec{k}}-E_d^{\text{vol}}}$$
$$+\left[\frac{\langle \vec{k}\mid \Delta_{\text{vol}}\mid \phi_d\rangle\langle \phi_d\mid \Delta_{\text{struc}}\mid \vec{k}\rangle+\text{c.c.}}{\epsilon_{\vec{k}}-E_d^{\text{vol}}}\right.$$
$$\left.-\frac{\langle \vec{k}\mid \Delta_{\text{vol}}\mid \phi_d\rangle\langle \phi_d\mid \delta V_{\text{struc}}\mid \phi_d\rangle\langle \phi_d\mid \Delta_{\text{vol}}\mid \vec{k}\rangle}{(\epsilon_{\vec{k}}-E_d^{\text{vol}})^2}+\cdots\right]\ , \tag{A4}$$

where we have expanded the denominator in powers of $\langle \phi_d\mid \delta V_{\text{struc}}\mid \phi_d\rangle$. The dots in Eq. (A4) represent (negligible) third- and higher-order terms. Writing out Δ_{struc} in terms of δV_{struc} and comparing the terms in large parentheses in Eq. (A4) with the definition of $h_2(\vec{k},\vec{r})$ in Eq. (22), leads immediately to the result

$$\mp N\frac{2\Omega_0}{(2\pi)^3}\int_{k\gtrless k_F}\sum_d\frac{\langle \vec{k}\mid \Delta\mid \phi_d\rangle\langle \phi_d\mid \Delta\mid \vec{k}\rangle}{\epsilon_{\vec{k}}-E_d}d\vec{k}=\mp N\frac{2\Omega_0}{(2\pi)^3}\left[\int_{k\gtrless k_F}[h_1(\vec{k},0)-\int h_2(\vec{k},\vec{r})\delta V_{\text{struc}}(\vec{r})d\vec{r}]d\vec{k}\right]\ . \tag{A5}$$

The final term in Eq. (A3) and the final term in Eq. (A5) then combine to give the net second-order contribution (35) from the structure dependence of the hybridization. Equation (A2) thus reduces to

$$\sum_\alpha \delta E_\alpha = N\frac{2\Omega_0}{(2\pi)^3}\left[\int_{k<k_F} w_0^{\text{pa}}(\vec{k},0)[1+p(\vec{k})]d\vec{k}\mp\int_{k\gtrless k_F} h_1(\vec{k},0)\left[1-\frac{w_0^{\text{pa}}(\vec{k},0)}{\epsilon_{\vec{k}}-E_d^{\text{vol}}}\right]d\vec{k}\right]$$

$$-n_{\rm unif}\sum_i v^i_{\rm pa}-\sum_i n^i_{\rm oh}\delta V^i_{\rm struc}+\frac{(Z^*-Z)}{Z}n_{\rm unif}(V_{unif}-\sum_i v^i_{\rm unif})+E_{\rm rest}\ . \tag{A6}$$

Using Eq. (A6) in Eq. (A1), subtracting and adding a term $\frac{1}{2}\delta n_{\rm oh}\delta V_{\rm oh}$, and using the following results:

$$-\sum_i n^i_{\rm oh}\delta V^i_{\rm struc}=\sum_{i,j}{}' n^i_{\rm oh}\left[\frac{Z}{Z_a}v^j_{\rm nuc}+v^j_{\rm nuc\text{-}core}\right]+\delta n_{\rm oh}\left[\delta V_{\rm val}+\frac{d\mu_{\rm xc}(n_{\rm unif})}{dn}\delta n_{\rm val}\right], \tag{A7}$$

$$(\delta n_{\rm oh}-\tfrac{1}{2}\delta n_{\rm val})\left[\delta V_{\rm val}+\frac{d\mu_{\rm xc}(n_{\rm unif})}{dn}\delta n_{\rm val}\right]-\tfrac{1}{2}\delta n_{\rm oh}\delta V_{\rm oh}$$
$$=-N\sum_{\vec q}{}'\,|S(\vec q)|^2\left[\frac{2\pi e^2\Omega_0}{q^2}\right]\{G(q)[n_{\rm oh}(q)]^2+[1-G(q)][n_{\rm scr}(q)]^2\}\ , \tag{A8}$$

and

$$E_{\rm es}(Z)+\tfrac{1}{2}\delta n_{\rm oh}\delta V_{\rm oh}+\frac{Z}{Z_a}\sum_{i,j}{}' n^i_{\rm oh}v^j_{\rm nuc}+n_{\rm unif}\sum_i(v^i_{\rm nuc\text{-}core}-v^i_{\rm pa})+\frac{(Z^*-Z)}{Z}n_{\rm unif}\left[V_{\rm unif}-\sum_i v^i_{\rm unif}\right]$$
$$=N[E^{\rm struc}_{\rm es}+E_{\rm oh}-\tfrac{3}{5}(Ze)^2/R_{\rm WS}]+\tfrac{1}{2}\sum_{i,j}{}' n^i_{\rm oh}\left[v^j_{\rm oh}-\frac{(Z^*-Z)}{Z_a}v^j_{\rm nuc}\right], \tag{A9}$$

leads immediately to Eqs. (43)–(52).

APPENDIX B

We summarize below simple analytic formulas derived from Eq. (78) and used to calculate various band energies in Tables I, II, and V. For the Γ point, retaining a single plane wave ($\vec G=0$) puts the bottom of the conduction band at

$$\Gamma_1=\langle 0\,|\,w_0\,|\,0\rangle\equiv w_0(0,0)\ , \tag{B1}$$

while the d-like $\Gamma_{25'}$ and Γ_{12} states in the fcc structure have energies

$$\Gamma_{25'}=E_d+3dd\sigma+4dd\pi+5dd\delta \tag{B2}$$

and

$$\Gamma_{12}=E_d+\tfrac{3}{2}dd\sigma+6dd\pi+\tfrac{9}{2}dd\delta\ . \tag{B3}$$

The quantities $dd\sigma$, $dd\pi$, and $dd\delta$ represent the $m=0,1$, and 2 components of the integral $-\Delta^{ij}_d$, as given by Eq. (53), with $|\vec R_i-\vec R_j|$ equal to the nearest-neighbor distance. The energy E_d marks the center of gravity of the unhybridized d bands and to a good approximation one finds in practice

$$E_d\cong\tfrac{3}{5}\Gamma_{25'}+\tfrac{2}{5}\Gamma_{12}\ . \tag{B4}$$

For the X point in the fcc structure, two plane waves ($|\vec G|=0,\ 4\pi/a$) are adequate in Eq. (78). Then one has

$$X_1=\tfrac{1}{2}[A(k_0)+E_d+D]\pm\{\tfrac{1}{4}[A(k_0)-E_d-D]^2+40\pi\Delta^2_{\rm vol}(k_0)\}^{1/2}\ , \tag{B5}$$

$$X_2=E_d-\tfrac{3}{2}dd\sigma+2dd\pi-\tfrac{9}{2}dd\delta\ , \tag{B6}$$

$$X_3=E_d+3dd\sigma-4dd\pi-3dd\delta\ , \tag{B7}$$

$$X_{4'}=B(k_0)\ , \tag{B8}$$

and

$$X_5=E_d-3dd\sigma-dd\delta\ , \tag{B9}$$

where we have defined $k_0=2\pi/a$,

$$D=\tfrac{1}{2}dd\sigma-6dd\pi+\tfrac{3}{2}dd\delta\ , \tag{B10}$$

$$A(k)=\epsilon_{\vec k}+w_0(\vec k,0)+w_0(\vec k,-2\vec k)\ , \tag{B11}$$

and

$$B(k)=\epsilon_{\vec k}+w_0(\vec k,0)-w_0(\vec k,-2\vec k)\ , \tag{B12}$$

with $w_0(\vec k,\vec q)$ and $\Delta_{\rm vol}(k)$ given by Eqs. (37) and (75), respectively.

Well outside of the d bands [i.e., $E(\vec k)\gg E_d$ or $E_d\gg E(\vec k)$], one may usefully fold down the secular determinant (78) into the plane-wave form

$$\left|\left|[\epsilon_{\vec k-\vec G}-E(\vec k)]\delta_{\vec G\,\vec G'}+\langle\vec k-\vec G\,|\,w_0\,|\,\vec k-\vec G'\rangle+\sum_d\frac{\langle\vec k-\vec G\,|\,\Delta_{\rm vol}\,|\,\phi_d\rangle\langle\phi_d\,|\,\Delta_{\rm vol}\,|\,\vec k-\vec G'\rangle}{E(\vec k)-E_d}\right|\right|=0\ , \tag{B13}$$

where now only the reciprocal-lattice vectors $\vec{G}$ and $\vec{G}'$ are spanned. Equation (B13) can be used to obtain the following band energies at the L point in the fcc structure, retaining two plane waves ($|\vec{G}|=0, \sqrt{3}\,2\pi/a$):

$$L_1=\tfrac{1}{2}[A(k_1)+E_d]^2\pm\{\tfrac{1}{4}[A(k_1)-E_d]^2 +40\pi\Delta_{\rm vol}^2(k_1)\}^{1/2} \quad \text{(B14)}$$

and

$$L_{2'}=B(k_1)\,, \quad \text{(B15)}$$

where $k_1=\sqrt{3}\pi/a$. In Eq. (B14) the plus sign is for $\epsilon_F>E_d$ and is appropriate for the upper L_1 state in filled-d-band metals, while the minus sign is for $E_d>\epsilon_F$ and is appropriate for the lower L_1 state in empty-d-band metals.

In the simple-metal limit, $\Delta_{\rm vol}=dd\sigma=dd\pi -dd\delta=0$ and the X_1 and L_1 levels of interest are given by

$$X_1=A(k_0) \quad \text{(B16)}$$

and

$$L_1=A(k_1)\,. \quad \text{(B17)}$$

Finally, the true Fermi level E_F can be approximately calculated to first order as

$$E_F\cong\epsilon_F+\langle\vec{k}_F\,|\,w_0\,|\,\vec{k}_F\rangle +\sum_d\frac{\langle\vec{k}_F\,|\,\Delta_{\rm vol}\,|\,\phi_d\rangle\langle\phi_d\,|\,\Delta_{\rm vol}\,|\,\vec{k}_F\rangle}{\epsilon_F-E_d}$$
$$=\epsilon_F+w_0(\vec{k}_F,0)+h_1(\vec{k}_F,0) \quad \text{(B18)}$$

for empty- and filled-d band metals and as $E_F\cong\epsilon_F$ for partially-filled-d-band metals with a self-consistent valence.

---

*Permanent address after September 1, 1982.

[1]J. A. Moriarty, Phys. Rev. B 1, 1363 (1970).

[2]J. A. Moriarty, Phys. Rev. B 5, 2066 (1972).

[3]J. A. Moriarty, Phys. Rev. B 6, 1239 (1972).

[4]J. A. Moriarty, Phys. Rev. B 6, 4445 (1972).

[5]J. A. Moriarty, Phys. Rev. B 8, 1338 (1973).

[6]J. A. Moriarty, Phys. Rev. B 10, 3075 (1974).

[7]J. A. Moriarty, Phys. Rev. B 16, 2537 (1977) (referred to as paper I in the text).

[8]J. A. Moriarty, Phys. Rev. B 19, 609 (1979).

[9]W. A. Harrison, *Pseudopotentials in the Theory of Metals* (Benjamin, New York, 1966).

[10]V. Heine and D. Weaire, in *Solid State Physics,* edited by F. Seitz, D. Turnbull, and H. Ehrenreich (Academic, New York, 1970), Vol. 24.

[11]W. Kohn and L. J. Sham, Phys. Rev. 140, A1133 (1965).

[12]W. A. Harrison, Phys. Rev. 181, 1036 (1969).

[13]L. Dagens, J. Phys. F 6, 1801 (1976).

[14]L. Dagens, J. Phys. F 7, 1167 (1977).

[15]L. Dagens, Phys. Status Solidi B 84, 311 (1977).

[16]J. C. Upadhyaya and L. Dagens, J. Phys. F 8, L21 (1978).

[17]J. C. Upadhyaya and L. Dagens, J. Phys. F 9, 2177 (1979).

[18]V. L. Moruzzi, J. F. Janak, and A. R. Williams, *Calculated Electronic Properties of Metals* (Pergamon, New York, 1978) (referred to as MJW in the text).

[19]Several minor differences in notation between paper I and the present work should be mentioned. The localized inner-core and d states are now written as ϕ_c and ϕ_d, instead of φ_c and φ_d. The orthogonalization-hole quantities $n_{\rm oh}$ and Z^* in paper I are here denoted as $n_{\rm oh}^0$ and Z_0^*, respectively. In addition, the present definition of $h_2(\vec{k},\vec{q})$ is a factor of 2 larger than that of Eq. (55) of paper I. (There is also a typographical error in the latter equation: The correct exponential entering the final term is $e^{-i\vec{q}\cdot\vec{r}}$.) Finally, the volume energy terms $E_{\rm fe}^0$, $E_{\rm fe}$, and $E_{\rm vol}=E_{\rm fe}-E_{\rm fe}^0$ in paper I are here redefined as $E_{\rm fe}$, $E_{\rm vol}$, and $E_{\rm vol}-E_{\rm fe}$, respectively.

[20]R. W. Shaw and W. A. Harrison, Phys. Rev. 163, 604 (1967).

[21]The experimental binding energy is equal to the cohesive energy plus the energy required to ionize the Z valence electrons in the free atom. The experimental cohesive energies were taken from Ref. 22 and the experimental ionization energies from the *Handbook of Chemistry and Physics,* 56th ed. (CRC, Cleveland, 1975), p. E-68.

[22]C. Kittel, *Introduction to Solid State Physics,* 5th ed. (Wiley, New York, 1976).

[23]W. B. Pearson, *Handbook of Lattice Spacings and Structures of Metals* (Pergamon, New York, 1967).

[24]C. Rottman and J. B. VanZytfeld, J. Phys. F 9, 2049 (1979).

[25]A. Jayaraman, W. Klement, Jr., and G. C. Kennedy, Phys. Rev. 132, 1620 (1963).

[26]N. E. Cusack, Rep. Prog. Phys. 26, 361 (1963).

[27]O. K. Andersen, Phys. Rev. B 12, 3060 (1975); O. K. Andersen and O. Jepsen, Physica 91B, 317 (1977).

[28]A. K. McMahan (private communication).

[29]Equation (70) is the same condition that applies to a transition-metal impurity placed in a simple-metal

host. In the impurity problem, however, Z refers to the host and Z_d to the impurity and the two are not directly related.

[30]In the equations of Sec. II, the simple-metal limit is obtained by setting $\Delta=\Delta_{\rm vol}=0$ if the d states are occupied and $\phi_d=0$ if the d states are unoccupied.

[31]D. G. Pettifor, Phys. Rev. B 2, 3031 (1970); J. Phys. C 2, 1051 (1969).

[32]J. M. Ziman, Philos. Mag. 6, 1013 (1961).

[33]N. W. Ashcroft and J. Lekner, Phys. Rev. 145, 83 (1966).

[34]C. N. J. Wagner, H. Ochen, and M. L. Joshi, Z. Naturforsch. 20A, 325 (1965).

[35]The most recent measurement of $a(q)$ in liquid Cu is reported by O. J. Eder, E. Erdpresser, B. Kunsch, H. Stiller, and M. Suda, J. Phys. F 10, 183 (1980).

[36]L. Dagens, M. Rasolt, and R. Taylor, Phys. Rev. B 11, 2726 (1975).

[37]H. G. Smith, G. Dolling, R. M. Nicklow, P. R. Vijayaraghavan, and M. K. Wilkinson, *Proceedings of the IAEA Symposium on Inelastic Neutron Scattering* (IAEA, Vienna, 1968).

[38]A. D. B. Woods, B. N. Brockhouse, R. H. March, A. T. Stewart, and R. Bowers, Phys. Rev. 128, 1112 (1962).

[39]R. A. Cowley, A. D. B. Woods, and G. Dolling, Phys. Rev. 150, 487 (1966).

[40]G. Dolling and J. Meyer, J. Phys. F 7, 775 (1977).

[41]J. R. D. Copley and B. N. Brockhouse, Can. J. Phys. 51, 657 (1973).

[42]R. M. Nicklow, G. Gilat, H. G. Smith, L. J. Raubenheimer, and M. K. Wilkinson, Phys. Rev. 164, 922 (1967).

[43]W. A. Kamitakahara and B. N. Brockhouse, Phys. Lett. 29A, 639 (1969).

[44]J. W. Lynn, H. G. Smith, and R. M. Nicklow, Phys. Rev. B 8, 3493 (1973).

[45]R. Stedman and G. Nilsson, Phys. Rev. 145, 492 (1966).

[46]M. A. Coulthard, J. Phys. C 3, 820 (1970).

[47]B. N. Brockhouse, T. Arase, G. Caglioti, K. R. Rao, and A. D. B. Woods, Phys. Rev. 128, 1099 (1962).

[48]C. S. Barrett, Acta Crystallogr. 9, 671 (1956); D. L. Martin, Proc. R. Soc. London Ser. A 254, 433 (1960).

[49]J. A. Moriarty (unpublished).

[50]J. A. Moriarty, Solid State Commun. 31, 881 (1979).

[51]J. A. Moriarty and A. K. McMahan, Phys. Rev. Lett. 48, 809 (1982).